Thomas Gamper, BSc.

Digital reconstruction of 3D rock slope surface topology using open-source photogrammetric Methods

Master's Thesis
Submitted in fulfilment of the requirements for the degree of

Master of Science, MSc

Masterstudium Erdwissenschaften

at

Graz University of Technology

Ao.Univ.-Prof. Dr. Liu, Qian

Institute of Applied Geosciences
Graz University of Technology

Graz, December 2019

EIDESSTATTLICHE ERKLÄRUNG

AFFIDAVIT

Ich erkläre an Eides statt, dass ich die vorliegende Arbeit selbstständig verfasst, andere als die angegebenen Quellen/Hilfsmittel nicht benutzt, und die den benutzten Quellen wörtlich und inhaltlich entnommenen Stellen als solche kenntlich gemacht habe. Das in TUGRAZonline hochgeladene Textdokument ist mit der vorliegenden Masterarbeit identisch.

I declare that I have authored this thesis independently, that I have not used other than the declared sources/resources, and that I have explicitly marked all material which has been quoted either literally or by content from the used sources. The text document uploaded to TUGRAZonline is identical to the present master‘s thesis.

Datum / Date	Unterschrift / Signature

Acknowledgements

I would like to thank all the people that supported me doing this work.
My supervisor, Ao.Univ.-Prof. Dr. Liu Qian, for being patient when my time was short and I could not keep progressing for the Thesis, but also for always taking his time if I needed support or help in any way. And also my fellow geology students, Philipp Danzel, Christian Gögele and Thomas Schnedlitz, for giving me one or another tip on how to approach the different problems that appeared.
And last but not least I would like to thank my entire family for giving me the opportunity to fulfil this goal of mine, and supporting me in every way possible.

Table of contents

Abstract 1

1. Introduction 3

1.1. Problem statement ... 3
1.2. Review of previous approaches ... 4
1.3. Objectives of this work ... 5
1.4. Geological Overview ... 6
1.5. Gargazzone Fm. ... 7

2. Methodology 10

2.1. Geotechnical Basics ... 10
2.1.1. Discontinuities ... 10
2.1.2. Describing discontinuities ... 12
2.1.3. Bias for sampling and possibilities to avoid them ... 14
2.1.4. Picture quality and camera characteristics ... 14
2.2. Structure from motion basics ... 15
2.2.1. Structure from motion workflow ... 15
2.2.2. Production of the sparse point cloud ... 19
2.2.3. Production of the dense point cloud, Clustering views for Multi View Stereo (CMVS) ... 19
2.3. Georeferencing using SfM_georef ... 21
2.4. Field data Collection ... 22
2.5. Camera parameters ... 25
2.6. Processing surface cloud and its geo referencing ... 25
2.7. Digital extraction discontinuity characteristics ... 27

3. Results 31

3.1. Outcrop: Windlahn ... 31
3.2. Outcrop Halbweg ... 36
3.3. Outcrop: Alte Sarnerstrasse 1 ... 43
3.4. Outcrop: Alte Sarnerstrasse 2 ... 49
3.5. Computing efficiency ... 52
3.6. Statistical parameters of all outcrops ... 53
3.6.1. Results of orientation measurements ... 54

3.7. Comparison of the way the pictures were taken 56

4. Discussion **57**

5. Conclusions **58**

6. Bibliography **60**

List of figures

Figure 1: Geological map of the north-western sector of the Athesian volcanic group; edited from Brandner et al.(2016) 6
Figure 2: Left; Streckeisen diagram for classification of volcanic rocks. The rhyodacitic rocks of the Gargazzone Fm. plot inside the read area, edited from Le Maitre et al. (2002)..... 8
Figure 3: Left; close up view of the mineral structure of the rhyodacitic rocks, with the clearly visible “salami” structure caused by the amorphous rock mass with small phenocristalls (whitedots)..... 9
Figure 4: Close up if a heavily altered fracture (Outcrop Halbweg) 9
Figure 5: Overview of the typical discontinuities found described in all 4 outcrops for the Gargazzone Fm. That are at least two sets of very steep (sometimes vertical), very persistent discontinuities with one on top and additionally fractures. This creates rectangular blocks, often taking the form of big slabs. 11
Figure 6: Rock mass description and the geometrical properties; from Hudson et al. (1992)..... 12
Figure 7: Comparison of a scanline (left) and a tracemap (right)..... 13
Figure 8: Example set of detected SIFT features. Each detected SIFT feature is displayed as a black box centered on the detected feature location. SIFT detects a canonical scale and orientation for each feature, depicted by scaling and rotating each box; from Snavely et al. (2008) 16
Figure 9: Workflow from the field work to the results 17
Figure 10: A keypoint descriptor is created by first computing the gradient magnitude and orientation at each image sample point in a region around the keypoint location, as shown on the left. These are weighted by a Gaussian window, indicated by the overlaid circle. These samples are then accumulated into orientation histograms summarizing the contents over 4x4 subregions, as shown on the right, with the length of each arrow corresponding to the sum of the gradientmagnitudes near that direction within the region. This figure shows a 2x2 descriptor array computed from an 8x8 set of samples; from Lowe (2004)..... 18
Figure 11: Example of the clustered point cloud of Windlahn, on top the single outputs generated by the SfM-CMVS workflow creating the whole point cloud on bottom, merged with Cloud Compare. Since this dense point cloud was relatively small (8 million points) only three smaller clusters were created. 20
Figure 12: The blue point represent SfM features recognized by the SfM georef program, those are used to transform the point cloud..... 21
Figure 13: Example of Ground control points matching, using SfM_georef. The red crosses are the manually selected GCPs inside the picture, the blue circles indicate the position of the GCPs after the transformation..... 22
Figure 14: Screenshot of the noted GPS information for the outcrop Alte Sarnerstrasse 1, using the free app Geopaparazzi ©..... 23
Figure 15: Measurement of the Orientation using the app geoClino..... 23
Figure 16: Left; Measurements of the dimensions of the box..... 24

Figure 17: A sketch for coordinate transformation, the whole system get rotated and translated along all 3 axes. For the case of the orientation of the box only 2 rotations were needed, since it was put in horizontally to simplify this work step. 26
Figure 18: Transformation matrix used to generate the UTM coordinates using the in-situ measurements for Θ = dip and Ψ = dip direction. The transformation of the X axis can be avoided, since the measurement of dip and dip direction always are made relative to a horizontal line. 27
Figure 19: Measurements of the orientation of the discontinuities using the CloudCompare Compass tool (example from Alte Sarnerstrasse 2) 28
Figure 20: An example of the second approach to create a histogram of the measured one-point-thickness. Clearly visible is the peak at the 10 cm class. Not showing any other peaks that would clearly define other sets. 29
Figure 21: Example of extracting the discontinuity characteristics from the point cloud, the orientation was measured on the surfaces; meanwhile the normal distance got measured from a starting surface to each point of the other surfaces those surfaces 30
Figure 22: Orthphoto of the outcrop location along the access road to Windlahn, on the left of the picture (in yellow) is the national road S.S.508. 31
Figure 23: Panorama photo of the outcrop, the angles are distorted due to the panorama-projection. 32
Figure 24: Dense point cloud of the outcrop, the white patches is areas where vegetation covers the rock surface. On the bottom right a fresh breakout is clearly visible (reddish colour) that also follows the same joints as the other surfaces. 32
Figure 25: The four sets resulting with the CloudCompare analysis 33
Figure 26: Camera positions for Windlahn 33
Figure 27: Stereonet-plot of the measured set-orientations. With the 95% confidence cone 34
Figure 28: Location of the Outcrop Halbweg, accessible via the main road S.S.508, next to the river Talfer 36
Figure 29: Positions of the pictures taken, the different standing points are each forming big cones. 37
Figure 30: Overview of the outcrop. The picture is taken parallel to the subvertical discontinuities of the set 1, showing well their orientation and persistence through the rock mass. 37
Figure 31: Results of the Hough normal, created a scalar field for dip-direction. 38
Figure 32: Pointcloud of the outcrop, the areas without information are vegetation (on the bottom right), and caused by the orientation of the surface (left side). Latter could be changed by taking more pictures from an elevated point of view to the left, unfortunately there was no such place. 38
Figure 33: Stereonet of the Outcrop. 39
Figure 34: Close up of the outcrop, the wet patches are clearly visible on the righter side. But also other parts had changing surface colours 40
Figure 35: Comparison of the two separately generated point clouds for the outcrop Halbweg. The colour of the scalar field simply represents the different clusters created during the creation of the dense point cloud. On top there is the first iteration with 6 “sub-clouds” merged together, on bottom the second version with only 4 “sub-clouds” creating the full, dense point cloud. 41
Figure 36: On top is the coloured point cloud of the first calculations, in the middle the point cloud to compare. On the right side the transformation matrix, between the two clouds. The

scaling is almost perfectly, with only a small shift in the different axes (last column, values are in cm). 42
Figure 37: Orthophoto of the area around the outcrops Alte Sarnerstrasse 1 and Alte Sarnerstrasse 2 43
Figure 38: Top; overview picture of the outcrop, most noticeable is the drainage duct in the middle. Bottom; Detail of a highly fractured zone at the upper edge of the outcrop ..... **Fehler! Textmarke nicht definiert.**
Figure 39: The top figure shows all the camera positions for the Outcrop Alte Sarnerstrasse 1: showing a continuous row of face-on pictures and a closer row of pictures with an oblique angle, trying to capture the point sets perpendicular to the surface. 45
Figure 40: Top: Results for the approach with all the pictures taken for the Outcrop Alte Sarnerstrasse 1; the cloud shows sparse areas only at the edges and on surfaces orientated upwards (not caught by the camera). 46
Figure 41: Scalar field of the outcrop, only the data from the chosen sets are plotted. The area on the left of the drainage duct shows clearly a less defined surface. This rough appearance is due to the surface being highly fractured combined with thin spacing 47
Figure 42: Transformation matrix between the point cloud using all pictures and the point cloud using only 100 pictures 47
Figure 43: Stereonet for the outcrop Alte Sarnerstrasse 1 48
Figure 44: Point cloud of the outcrop, on the bottom right the box used for geo-referencing is clearly visible 49
Figure 45: Camera positons for the outcrop Alte Sarnerstrasse 2, on the top left side the additional camera angle is well visible, and on the left edge some sparse point are visible, that went cut out for the later work with the point cloud. 49
Figure 46: Comparison of the information given by the scalar field. On the bottom there is the full spectrum of dip-directions for the cloud. On top are the three sets extracted from the whole cloud. On a special note: it's important to not use the information of the wooden box, which is also clearly visible in both point clouds 50
Figure 47: Stereographic plot of the measured orientations 51
Figure 48: Time needed for the dense cloud reconstruction plotted vs the amount of points of that cloud 53
Figure 49: Two orientation measurements with different sample size using Cloud Compare compass on the same discontinuity surface, the left measurement with a big surface area being 54/286 and on the right with a small sampling area 66/275. 54

Abstract

The field work is the first step of many many tasks of a geologist; it is of crucial importance to get the information needed for all later work steps. Therefore every concept of improving this part of the work is very useful. Taking pictures of outcrops and interesting observations is already an approved tool, by going a step further and using photogrammetry there are a lot more possibilities, by not just taking pictures and panoramas, but by creating a georeferenced and scaled point cloud. This point cloud represents the observations like a snap of that outcrop of that exact moment. This thesis takes that idea and puts it to the test, creating an entire workflow from the field work, up to the data extraction in front of the PC. Since the structure from motion workflow has already been tested for different task and applications, this paper focuses on a cost efficient approach, meaning that all the used software programs are open source and therefore available to everybody.

In the field 4 different outcrops inside of the volcanic rocks of the Athesian volcanic group were chosen with a size of around 10 m length and 2-5 m height and roughly 150-200 images were shot with a digital single-lens reflex (DSLR) camera for each outcrop. This was done with different approaches of camera positioning. In the next step the point cloud was created using the software VisualSfM, created by Wu (2013). The point cloud was then orientated, scaled and georeferenced using SfM georef, created by James et al. (2012). All of this resulted in a dense point cloud of around 7-12 million points, recreating the outcrop in a digital working environment.

Working on that basis it is possible to gather data from that point cloud, in this case the main focus is on dip direction and dip of the discontinuities and their spacing. To be able to do that, the also freely available software CloudCompare was used. For the measuring of the orientation of the discontinuities the program Openstereo, created by Grohman et al. (2010) was used.

The results showed well defined properties for the distinctive sets of discontinuities, with a very efficient time management, the most time being consumed during the creation of the point cloud (no attendance at PC needed) and at for the data extraction of said point cloud. All in all the whole process can be done in less than a work day. Creating a repeatable result for each outcrop with a very fast fieldwork, this is especially interesting for outcrops that are unsafe or even just hard to reach with the state of the art approach with compass and scanline.

Die Feldarbeit ist der erste Schritt von vielen Aufgaben eines Geologen; es ist von entscheidender Bedeutung, denn alle späteren Arbeitsschritte bauen auf diese im Feld gewonnenen Informationen auf. Daher ist jedes Konzept zur Verbesserung dieses Teils der Arbeit von großer Bedeutung. Das Fotografieren von Aufschlüssen und interessanten Beobachtungen ist bereits ein bewährtes Werkzeug, durch den nächsten Schritt, die Photogrammmetrie, gibt es viel mehr Möglichkeiten, indem man nicht nur Bilder und Panoramen macht, sondern eine georeferenzierte und skalierte Punktwolke erstellt. Diese Punktwolke stellt die Beobachtungen wie eine Momentaufnahme des Beobachtungszeitpunkts dar. Diese Arbeit stellt diese Idee auf den Prüfstand und erstellt einen kompletten Workflow von der Feldarbeit bis zur Datenextraktion vor dem PC. Da die Struktur des Bewegungs-Workflows bereits für verschiedene Aufgaben und Anwendungen getestet wurde, konzentriert sich diese Arbeit auf einen kosteneffizienten Ansatz, d.h. alle verwendeten Softwareprogramme sind „Open Source“ und damit für jeden verfügbar.

Im Gelände wurden 4 verschiedene Aufschlüsse innerhalb der Vulkangesteine der Etschtaler Vulkanitgruppe mit einer Größe von ca. 10 m Länge und 2-5 m Höhe ausgewählt und ca. 150-200 Bilder mit einer digitalen Spiegelreflexkamera (DSLR) für jeden Aufschluß aufgenommen. Dies geschah mit verschiedenen Ansätzen der Kamerapositionierung. Im nächsten Schritt wurde die Punktwolke mit der von Wu (2013) entwickelten Software VisualSfM erstellt. Die Punktwolke wurde dann mit SfM-Georef, erstellt von James et al. (2012), im Raum orientiert, skaliert und georeferenziert. All dies führte zu einer dichten Punktwolke von jeweils rund 7-12 Millionen Punkten, diese erzeugen einen „virtuellen Aufschluss“.

Auf dieser Basis ist es möglich, Daten aus dieser Punktwolke zu sammeln, in diesem Fall liegt der Schwerpunkt auf dem Einfall und der Einfallsrichtung der Diskontinuitäten und deren Abstand. Um dies zu ermöglichen, wurde das ebenfalls frei verfügbare Programm CloudCompare verwendet. Für die Messung der Orientierung der Diskontinuitäten wurde das von Grohman et al. (2010) erstellte Programm Openstereo verwendet.

Das Resultat sind gut definierte Eigenschaften für die markanten Gesteinsoberflächen mit einem sehr überschaubaren Zeitmanagement, wobei die meiste Zeit bei der Erstellung der Punktwolke (keine Anwesenheit am PC erforderlich) und bei der Datenextraktion der Punktwolke verbraucht wurde. Alles in allem kann der gesamte Prozess in weniger als einem Arbeitstag durchgeführt werden. Dies ist besonders interessant für Aufschlüsse, die mit dem traditionellen Ansatz mit Kompass und Scanline unsicher oder gar schwer zu erreichen sind.

1. Introduction

1.1. Problem statement

Geology as a natural science tries to describe the nature, but to communicate with other fields like engineering it's important to put numbers on those observations to describe the different properties found in nature. The idea behind this concept has never changed, yet the methods to do so change over time. This is due to new ideas and concepts and also due to new technologies. It is an important task of science to test new methods and to try to adapt them for the goal needed. The last major change in the workflow of the geologists, the digitalization of the field work, is still in process. Only with the technological improvements made in the last decades it is possible to capture the complex character of nature using cameras and computers.

Defining rock mass properties in the field is quite a difficult task; a lot of experience and time is crucial to get a good result, but even then it is very important to be able to discuss and compare the results with other experts. For now the way-to-go approach is a scanline and the fastidious work that comes with it. One main problem here is that it is also very important to get a result that can be verified, repeated and re-interpreted by others. Once a scanline gets removed it is very difficult to recreate the same scanline on the original position, therefore precluding to recreate the fieldwork, making it difficult to check the data if some errors or problems with the original data appear. In the worst case, the entire work needs to be redone from scratch, starting with the fieldwork.

Yet another problem of the scanline is the limitation in space. Large outcrops can be, timewise inefficiently, handled by leaving the scanline in position and work for longer time periods, and by attaching one scanline behind another. But not just the size can be hard to handle, even the positioning; for example for an outcrop in a height of 15 m it is almost impossible to put a scanline, in a save mode without an enormous time investment. The other problem of putting scanlines is simply the pure danger, thinking of areas characterized by rockfall events or also in caves or during the building of a tunnel. In such areas it's rather unsafe to put a scanline until the entire surface is protected or retained by safety measurements. Creating a saver and faster method to gather data from such areas should be of great interest, even more so if the new method proves to be faster as well.

1.2. Review of previous approaches

Different approaches to tackle this problem were made, especially since the up rise of the digital age. One of the most common ways to describe the properties of nature is by recreating it as closely as possible, in the past this had to be done by creating detailed drawings and sketches but the modern method is done by creating a point cloud.

This can be done using different methods; of special interest is a method freely available to everyone, called SfM (Structure from Motion) by Furukawa et al. (2010). A typical point cloud is a representation of the surface of any given object, depending on the method used it additionally gives information about the colouring (RGB) of that surface. Starting from this point cloud it is possible to measure the properties of the captured outcrop in a virtual environment.

Snavely (2008) made a big effort on using the structure from motion tool on a big scale, by using it to recreate 3D models. As input he chose to use hundreds of freely available pictures from the internet to generate point clouds of famous places around the world. He proved that the SfM tool works with a huge amount of unstructured and highly diverse sets of images, showing that there are enormous possibilities when it comes to applying this concept on images.

For the field of palaeontology Falkingham (2014) tested out the idea of point clouds to describe fossils, with big differences in scale, from a fem mm to a few meters, showing the methods strengths when it comes to easiness of use and flexibility on different scales.

James and Robson (2012) used the SfM workflow to generate topographical surfaces over large distances, while also comparing the results to traditional stereo-photogrammetry. They demonstrate the comparable accuracy between them, while showing the benefits of the SfM approach, being much more user-friendly and flexible. They also investigated the use of the free software investigating the cliff erosion, creating multiple point clouds on a coastal cliff while comparing it to a terrestrial laser scanner, there the big advantage is again the fast acquisition of data in the field.

Probably one of the most promising approaches to improve the SfM workflow and make it a basic tool for the future, is to combine it with small drones (Unmanned aerial vehicle – UAV), a method called UAV-based photogrammetry. By using this concept it is possible to create digital elevation models (DEMs). The paper of Bemis (2014) also shows a full workflow from setting the ground control points (GCPs) in the field to the final georeferenced, photorealistic model. Showing different possible uses and interpretations of the data, for example measuring en-echelon veins on a hand sample or using semi-automated processes to detect and define discontinuities on outcrops.

1.3. Objectives of this work

The main goal of this work is to create an entire workflow using SfM, from the field work to the data extraction and interpretation in the office. To make the whole process more interesting and revealing, all these steps were made, by using open source software, and a simple handheld DSLR (digital single-lens reflex) camera. The flexibility of the approach was proven by many other studies (see chapter 1.2) and this thesis goes a step further and tries to establish this workflow as a basic tool for each and every geologist going into the field.
Therefore the entire workflow was made with open source programs provided by many different instances.
Resulting in a sort of a field-test for geologist with a small budget. Another important aspect investigated is the time management for this method, the field work has shown to be very time efficient (e.g. Bemis et al., 2014; James et al., 2012). Therefore one goal is to see if it is possible to gather the, geologically speaking, most important parameters by using the quick field work with photogrammetry. Connected with this idea is also the idea of reducing the input of images, to see until what point the workflow gives valuable data. To get a better understanding on how well this works with different surfaces and sceneries. And lastly it's also crucial to see if there are possibilities to improve the whole process beginning from the first step of the field work to the data extraction of the final point cloud.

1.4. Geological Overview

All the outcrops are located in the Southern Alps, located north of Bolzano. From a geological point of view the outcrops are part of southalpine. The southalpine is part of the Apulia microplate, just like the Austroalpine, both are part of the continental margin and show a similar geodynamic development since the Lower Permian. The break-up of Pangea caused a continental rift which lead to pulses of distinct rifting tectonics in the dolomites. These processes are closely associated with the voluminous plutonic and volcanic rocks deposited in this area, (Brandner et al. 2016).

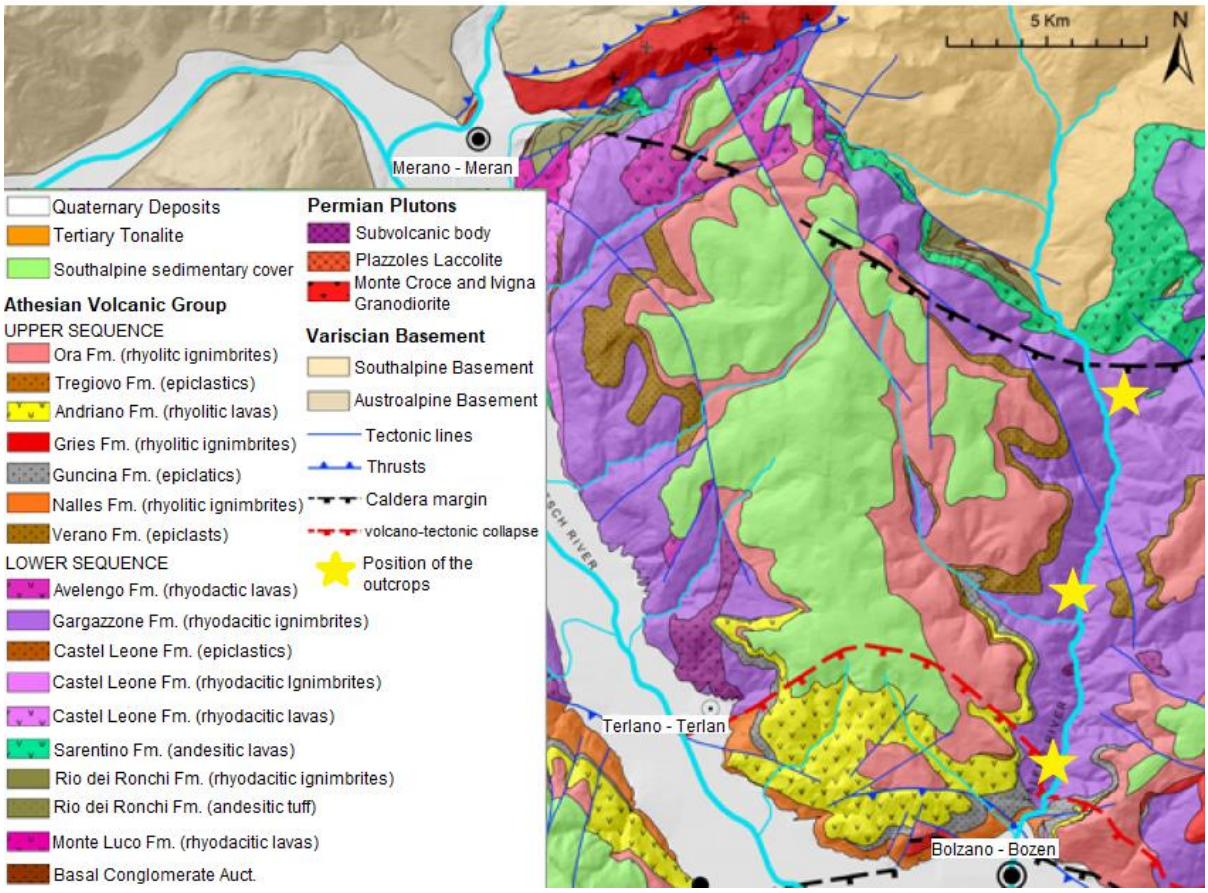

Figure 1: Geological map of the north-western sector of the Athesian volcanic group; edited from Brandner et al.(2016)

The volcanic rocks of the outcrops formed during the first of four tectonically controlled megacycles of the Permian-Triassic succession of the dolomites.

During the Early Permian volcanism the deposits were formed over a time span of ca. 10 Ma (285-275Ma before present), (Marocchi et al., 2008). These deposits fill up the Bolzano/Bozen basin and cover the Variscian crystalline basement, reaching a thickness up to 3 km. On the base of the volcanic sequence lies the Variscian basement, on top of the

Athesian group lies the Val Gardena sandstone. This tells the story of the collision forming the Alps; on base there is the old European basin, followed up by the volcanic sequences during the subduction and on top there are the relicts of the opening and infilling of the Thethys, a shallow intra-mountain basin, (Brandner et al., 2016).

These volcanic sequences are now called Athesian group, but were prior known as “Bozner Quarzporphyr”. The duration of the volcanic activity inside the sequence is determined based on radiometric U/Pb measurements with zircons. Its duration was around 15Ma years during the Permian, (Morelli, et al., 2013).

All the outcrops covered in this paper are inside this volcanic sequence, as shown in Fig. 1.

1.5. Gargazzone Fm.

The outcrops lie inside the Gargazonone Fm.; this Formation is formed by Ignimbrite-layers reaching thicknesses up to 400 (Sarntal) and 900m (Etschtal). From a petrologic point of view we are dealing with rhyodacitic Lapilli Tuff; often showing a strongly fluidal structure (Surge-deposit).

The QAPF diagram (Fig. 2), is used to describe rocks with little mafic mineral content, less than 10%, for it the volumetric percentage of the different mineral components are plotted in a ternary plot. The corners of the diagram are Q = quartz, A = alkali feldspar, P = plagioclase and F = feldspathoid (Le Maitre et al., 2002).

Bargossi (2011) describes the rocks of the Gargazzone Fm. for the official CARG map (sheet 013 Merano); they plot close to the Plagioclase and Quartz line, with little alkaline components. The mineral composition of the rock includes Quartz, Sanidine and Plagioclase, with minor components of Biotites and Amphibolites. The mineral texture is typical for porphyric (“salami structure”, Fig. 3) with a fine-grained matrix formed by the plagioclase minerals. The bigger grains, that are visible with the eye, are formed by Feldspar Minerals (for example Sanidine) or Quartz.

The colour of the rock is black to grey-greenish, due to oxidation this colour changes to a violently red. The rock mass is characterized by sub-vertical joints, breaking the rock mass down to regular shaped block with a platy form and a thickness of (1-30cm) (Bargossi et al., 2011).

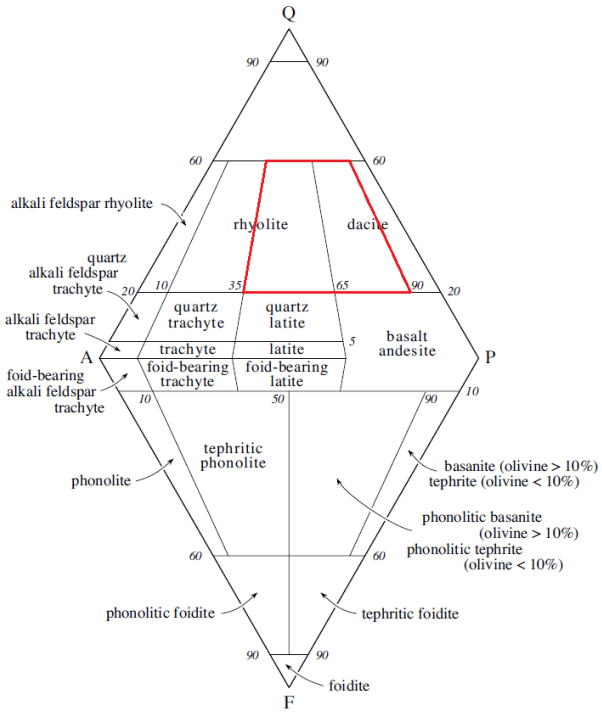

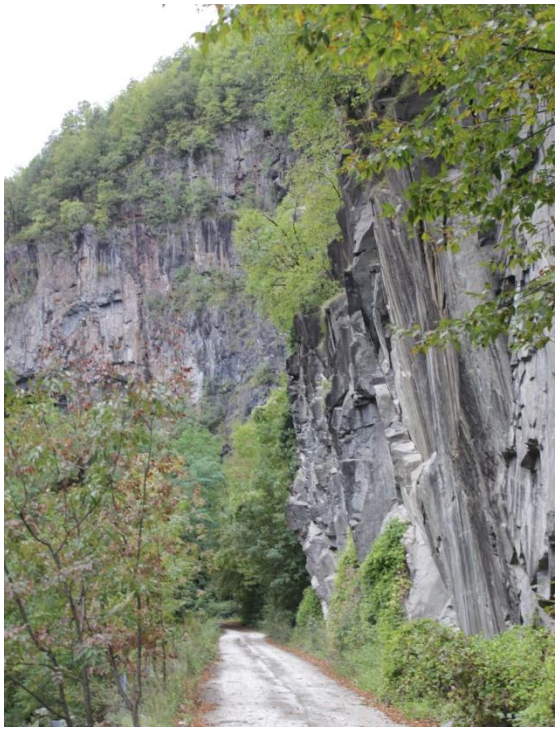

Figure 2: Left; Streckeisen diagram for classification of volcanic rocks. The rhyodacitic rocks of the Gargazzone Fm. plot inside the read area, edited from Le Maitre et al. (2002) Right; the walls of the gore close to the outcrop Halbweg (see chapter 3.2)

The rock-surface is smooth and only slightly altered, the discontinuities of the Ignimbrites are usually very persistent and penetrate the whole rock mass. The joints are usually closed with no infill (Fig. 4), unless they are exposed to surface processes, here it is quite common to find openings in the mm-range.

From a morphological point of view, very steep rock walls are typical for the Gargazzone Fm. (See Fig. 2 and Fig. 5). This is very well noticeable for the outcrop Halbweg (Fig. 5) but is generally true for this Formation. This also explains the morphological appearance of the Sarntal-gore, where all investigated outcrops are located. The valley is well known for the very steep walls, the old access road was also infamous for many dangerous parts with repeated rock falls.

Figure 3: Left; close up view of the mineral structure of the rhyodacitic rocks, with the clearly visible “salami” structure caused by the amorphous rock mass with small phenocristalls (whitedots)
Right; slightly altered surface next to a discontinuity.

Figure 4: Close up if a heavily altered fracture (Outcrop Halbweg)

2. Methodology

2.1. Geotechnical Basics

2.1.1. Discontinuities

Discontinuities split the intact rock up into different areas. This leads often to different properties and behaviour of the rock mass. By a simple approach the fracturing is caused by stress differences inside the rock, which leads to cracking. Typical discontinuities are bedding planes, foliation planes or joints, the latter two were caused by tectonic processes. Discontinuities and their properties are of crucial importance when it comes to describe the quality and expected behaviour of a rock mass. For a better understanding of the impact and the persistency of these discontinuities it is important to know the origins of fractures.

For the purpose of this thesis, three main sources are considered. The oldest and most persistent fractures have their origin in the genesis of the rock mass itself, since it is a thick geological unit of volcanic rock. After reaching the surface the cooling of the melted rock started. This happened vast and therefore not uniformly from top to bottom of the material leading to vertical stress differences inside the rock, the result of this are very persistent vertical discontinuities. These joints maybe were stressed further during the alpine orogenesis.

Secondly, after the exhumation of the investigated areas, the exposure to the weather allowed water to further increase the fracturing of the rock. The water infiltrates trough the existing joints and works its way deeper, meanwhile closer to the surface the water can freeze. While freezing the water increases in volume by roughly 10%, this increases the pressure on the fracture walls and loosens them up, or even creates new joints that are far less persistent than the tectonic ones.

Lastly there are the youngest joints that are of anthropogenic origin. Since the outcrops are very close to roads, during the building of these roads (especially the sites Alte Sarnerstrasse 1 and Alte Sarnerstrasse 2, Fig. 27 and Fig. 33) and to increase the safety, the rock surface was remodelled by excavators or other tools. This created new discontinuities which have the same orientation as the weakest part of the rock (natural discontinuities), but the spacing is a lot smaller. This joints generally don’t pose any danger of big rock falls, because the persistency of them is very shallow, often not even penetrating deeper than the rocks surface.

Figure 5: Overview of the typical discontinuities found described in all 4 outcrops for the Gargazzone Fm. That are at least two sets of very steep (sometimes vertical), very persistent discontinuities with one on top and additionally fractures. This creates rectangular blocks, often taking the form of big slabs.

2.1.2. Describing discontinuities

To gather information about discontinuities (Fig. 6 and Fig. 7) they have to be measured in some kind of way. Most established is the scanline-approach. A measuring tape is put next to the outcrop and then all intersecting discontinuities get captured, also the orientation of the tape has to be measured. For each discontinuity different properties are noted

- orientation α/β (dip/dip direction)
- fracture type
- spacing/ frequency
- semi trace length
- termination
- roughness/waviness
- surface alternation
- aperture/filling

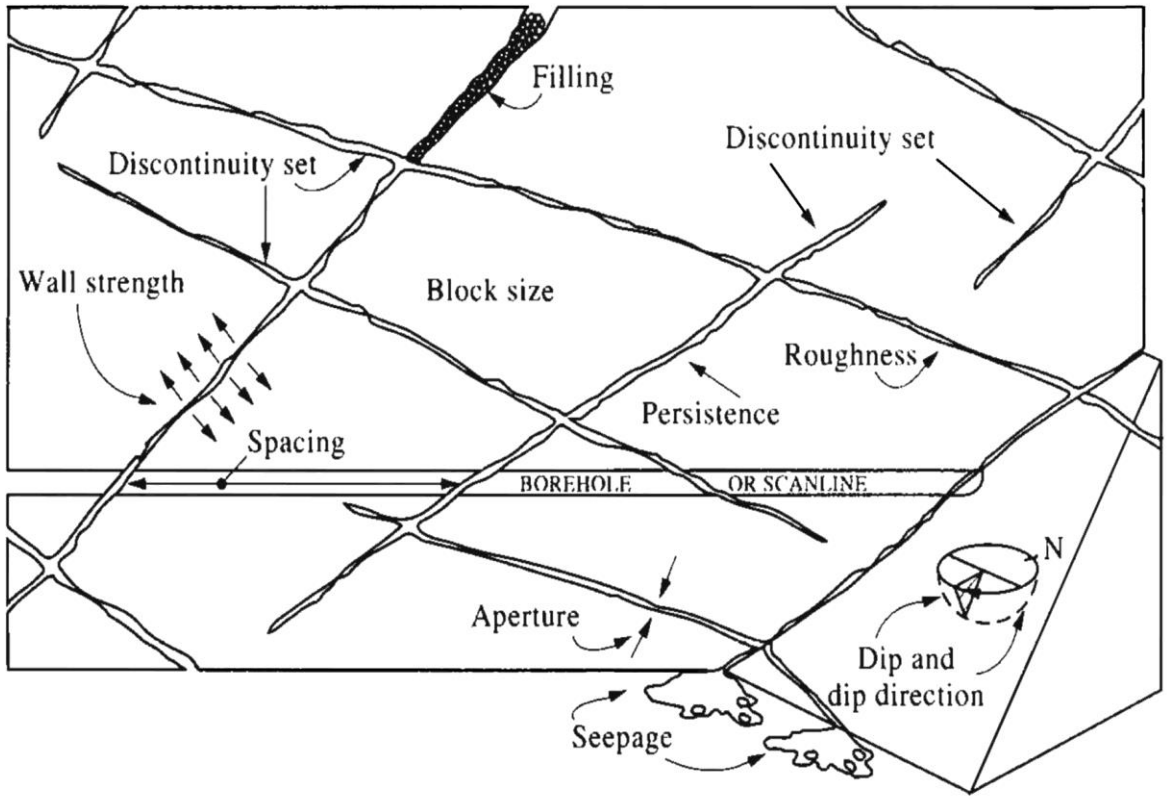

Figure 6: Rock mass description and the geometrical properties; from Hudson et al. (1992)

Another approach is the 2D-areal sampling, basically an extended scanline, where all discontinuities inside a sampling window are noted, the same data as with the scanline, but with the additional information about the mean trace length. This creates a so called trace map, additionally to the mean trace length this gives also valuable information about the distribution of discontinuities.

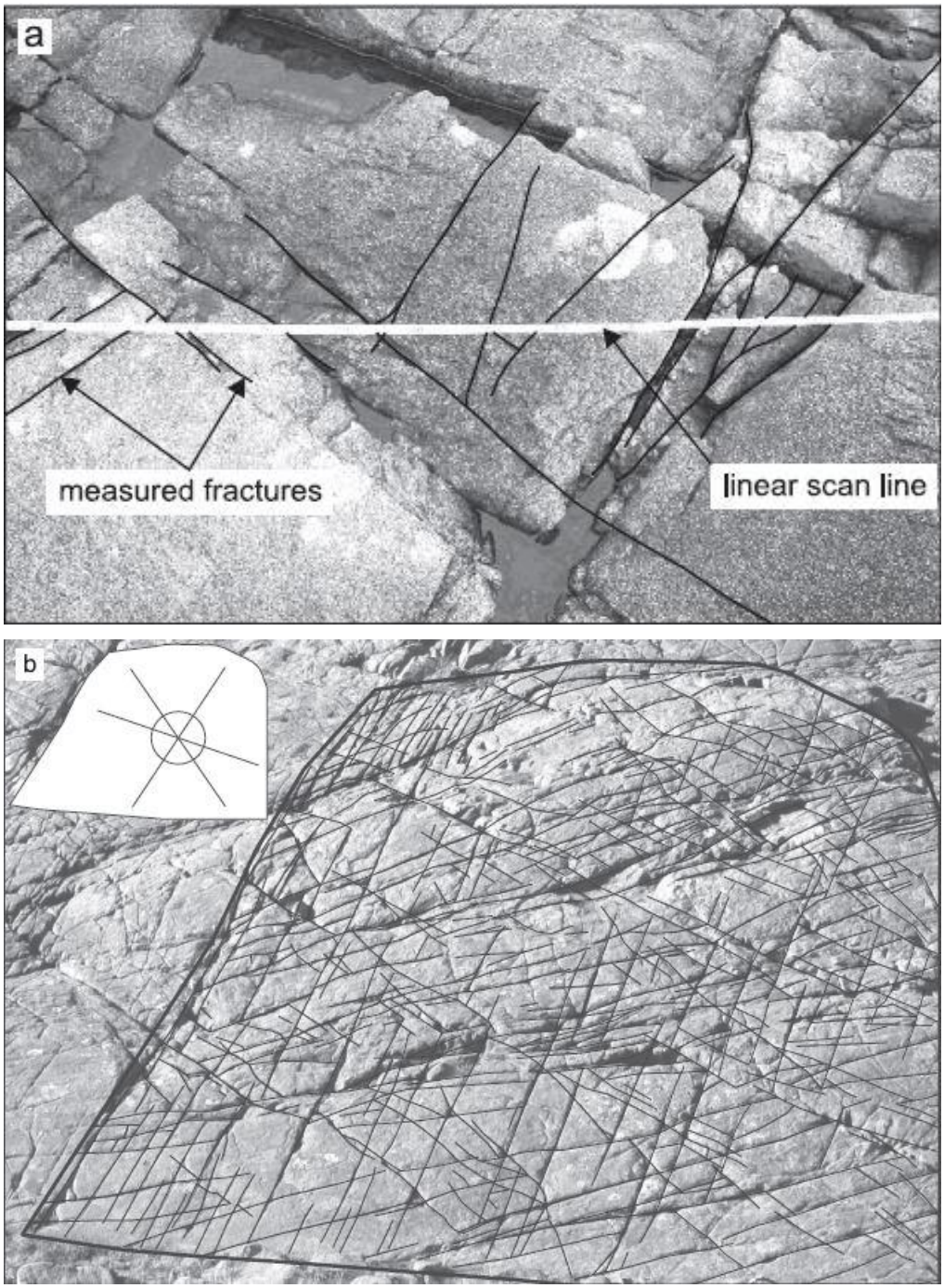

Figure 7: Comparison of a scanline (left) and a tracemap (right)
From Watkins et al. (2015)

For example in (Fig 7 bottom image) it is well visible that the discontinuities going left to right are locally much more concentrated, whilst the discontinuities going from bottom to the top are distributed quite uniformly.
Lastly there is the approach of the 3D-digital sampling, used in this thesis to describe the different outcrops. This approach gathers the most information of the outcrop in a fast way, nevertheless to get the needed information the data has to be processed and interpreted.

2.1.3. Bias for sampling and possibilities to avoid them

For all the approaches there is a certain bias, which has to be understood to not misread the gathered data.
The size bias is caused by the sampling (outcrop) size, large discontinuities are much more likely to appear than small sized ones. This is best avoidable if the sampling area is big enough.
The orientation bias on the other hand describes the problematic orientations for an outcrop, orientations that are parallel to the outcrop surface won't appear that many times than ones that are perpendicular to the surface. To reduce the effect of the orientation bias it's best to measure in multiple directions or at least be aware of the fact, that surface areas usually are also caused by discontinuities. Other biases are caused by the difficulty to measure trace lengths that are very small or extend far over the sampling area (Liu, 2018).

2.1.4. Picture quality and camera characteristics

Image optimization is a key parameter for the creation of high-quality point clouds. Especially if they are used later on to gather data like orientation or measurements of different distances.
Unlike traditional photogrammetry that relies heavily on the quality of ground control points (GCP), the accuracy of SfM is reliant on the properties of the image, like light, camera angle or distance. Therefore for the camera should be chosen in a way, to get the maximum of information of each data set. For resolution Mosbrucker (2017) considers an effective resolution of at least 16MP for SfM uses. When it comes to camera configuration, the two most important properties are exposure and focus. The exposure gets influenced by different factors; ISO, lens aperture and shutter speed.
All this parameters should be chosen for each site to create pictures with the greatest effective resolution.
The focal length tis another important property of the camera, for example fisheye lenses produces a lot more distortion, which causes problems for the SfM workflow (James et al., 2012)

2.2. Structure from motion basics

Structure from motion is a tool to generate 3D models from 2D imagery by using multiple algorithms (matching image texture in different photographs). The workflow is more commonly known as SfM-MVS (Structure from Motion- Multi-View Stereo) (Carrivick et al., 2016), see Fig. 8. The process considers the entire scene as static, this has to be considered for the field work; areas with strong shadows, diffuse light or heavily changing light conditions won't be reconstructed well. Also areas with no change in texture and colour (for example reflections) will be fleshed out poorly.
Ideally the ground control points (GCP) would be placed at the edges of the scene, so during the georeferencing transformation, the data does not need to be extrapolated (James et al. 2012).

2.2.1. Structure from motion workflow

First step of the SfM workflow is the feature detection, because it is the first step it is also the intersection of the field survey and the data analysis. Lots of progress was made in order to identify common points, this common points (or Keypoints) later allow matching different images together (Carrivick et al., 2016).
Logically the next idea is to use feature points, which are sets of pixels that are invariant to changes in scale and orientation and also invariant with the transformation. This has to be possible even with geometric distrotions due to different perspectives and camera angles between the pictures. This requires that the detected areas have a shape which is a function of the image. And therefore can be "recreated" by a movement of the camera (translation). More advanced region detectors also take changes in scale into consideration. For example the Difference of Gaussian (DoG), Lowe (2004) allows to search scale-independent regions. This is where the extracted image regions, the so called region descriptors, come to use, those allow to compute complex operations like wide baseline matching, object recognistion or robot localization.
The descriptor used by VisualSfM is a SIFT descriptor (Scale-invariant feature transform) (Lowe, 2004).
This descriptor is invariant to uniform scaling, orientation, illumination changes, and partially invariant to affine distortion (Remondino, 2006).

Carrivick (2016) splits the function of SIFT in four stages:

1. Detection of spatial extrema: The first step of SIFT is to identify locations and scales to a region from different viewpoints (see Fig. 8).
2. As second step the keypoints get localized, this is done by fitting a quadratic function for each possible keypoint to nearby data for scale, location and ratio of principal curves. The density of identified keypoints is highly reliant on the resolution of the image and the complexity of the surface texture. Rough surfaces with complex textures generate a lot more keypoint than for example a featureless white wall.
3. The orientation of each keypoint gets assigned using the Gaussian smoothed images closest to the scale of the keypoint. The Gaussian smoothing is usually used to blur images, the Gaussian outputs a `weighted average' of the neighbourhood of each pixel. The average is weighted more towards the value of the central pixels, this results in a smoothing with a relatively good preservation of edges (Fisher et al., 2000)
4. Finally a descriptor (Fig. 10) for each point is required that is sufficiently distinctive while being as invariant as possible to variations in perspective or illumination. To achieve this, a Gaussian weighting function gets applied. The purpose of this Gaussian window is to avoid sudden changes in the descriptor with small changes in the position of the window, and to give less emphasis to gradients that are far from the centre of the descriptor. Resulting in a descriptor that is a 4 × 4 array of histograms with eight orientation bins, each creating a 128-element feature vector for each keypoint Lowe (2004), see Fig 10.

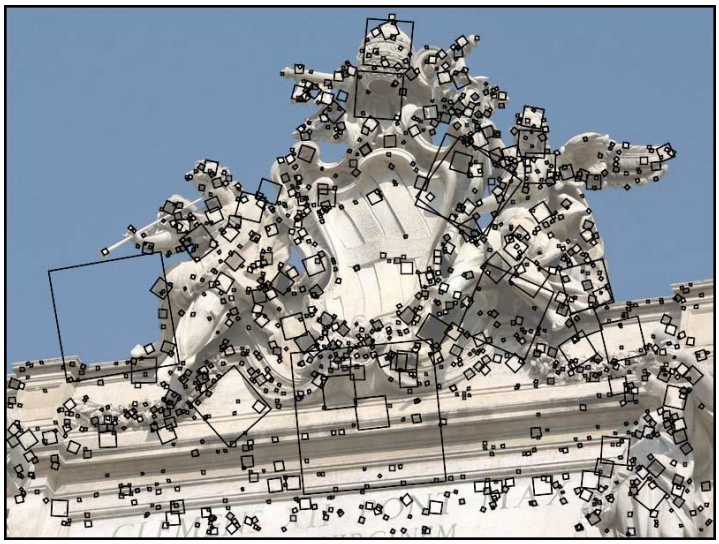

Figure 8: Example set of detected SIFT features. Each detected SIFT feature is displayed as a black box centered on the detected feature location. SIFT detects a canonical scale and orientation for each feature, depicted by scaling and rotating each box; from Snavely et al. (2008)

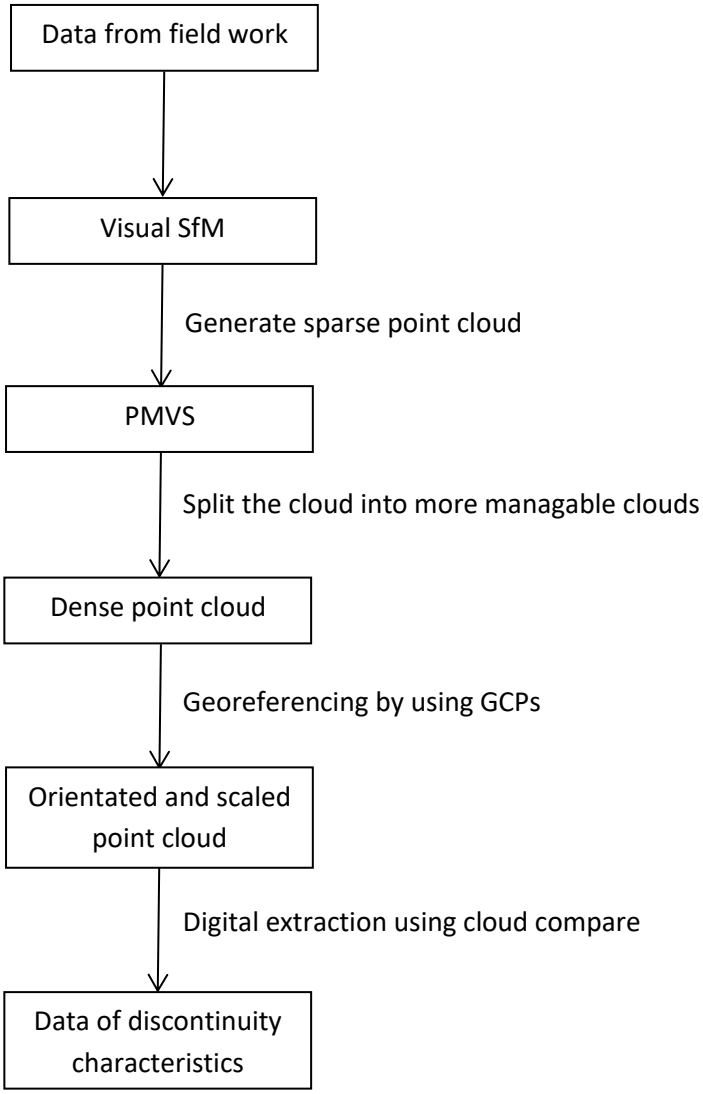

Figure 9: Workflow from the field work to the results

For now there are a lot of keypoints, in the next step a check is made, if the observed keypoint is located in other images, or if is possible to “drop” it. Therefore a new image gets matched by comparing each feature of the image to this previous database. Matching features are based on Euclidean distance of their feature vectors. This fast nearest-neighbour algorithm allows working with huge databases with a fast computation. Another way to fasten up the process is purposed by Lowe (2004) by stopping the approximate nearest neighbour (ANN) search after the first 200 nearest neighbour candidates; this saves time while only loosing less than 5% of correct matches (Lowe, 2004).

To eliminate the remaining incorrect keypoints another filter is applied, the so called fundamental matrix (F-Matrix). The relationship between two images gets constrained by

applying the eight-point algorithm (Longuet-Higgins, 1981). ‘This works by using eight-point matches on two uncalibrated views, a set of linear equations is used to reconstruct a scene up to a projective transformation, where all points that are found on a single line, will remain aligned (Carrivick et al., 2016).

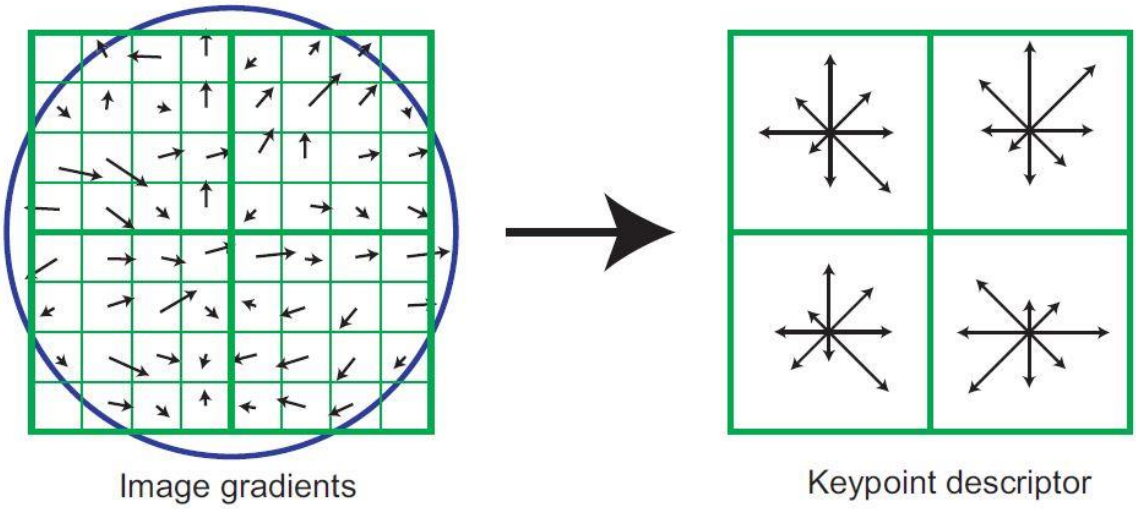

Figure 10: A keypoint descriptor is created by first computing the gradient magnitude and orientation at each image sample point in a region around the keypoint location, as shown on the left. These are weighted by a Gaussian window, indicated by the overlaid circle. These samples are then accumulated into orientation histograms summarizing the contents over 4x4 subregions, as shown on the right, with the length of each arrow corresponding to the sum of the gradientmagnitudes near that direction within the region. This figure shows a 2x2 descriptor array computed from an 8x8 set of samples; from Lowe (2004)

Possible F-Matrices run for several iterations, most popular using the random sample consenus (RANSAC). RANSAC divides all keypoints into two groups: inliers and outliers, and then tries to fit a model that ignores all outliers. A certain threshold has to be specified to define an inlier, this is set to be 0,6% of the maximum image dispersion (Snavely et al., 2008). The process starts by taking a sample of keypoints, they are used to calculate the F-Matrix, and additionally the number of inliers gets counted.

With the limitation of keypoints to these matches, a new form of organizing the links between every image pair can be put into place: the so called tracks. They use the library of images to connect sets of matching points (Snavely et al., 2008). A track has to have at least two keypoints in three images.

2.2.2. Production of the sparse point cloud

To create the sparse point cloud, the program Bundler (written in C and C++) uses the set of pictures, picture features and the image matches gathered in the previous steps to reconstruct the camera and scene geometry (Snavely et al., 2006).
In the first step, by using the gathered information it is now possible to reconstruct the orientations and the intrinsic camera calibration parameters. For the latter a camera calibration matrix (K) is used:

$$K = \begin{bmatrix} a_u & s & u_0 \\ 0 & a_v & v_0 \\ 0 & 0 & 1 \end{bmatrix}$$

$a_u; a_v \ldots \text{immage scale in X and Y direction}$

$s \ldots \text{skew}$

$u_0; v_0 \ldots \text{princioal point, location of intersection of image plane with optical axis}$

Those computations are formulated as nonlinear least squares problems, using the Levenberg–Marquardt algorithm. Provided with initial estimates, Bundle Adjustments (BA) simultaneously refines motion and structure by minimizing the reprojection error between the observed and predicted image points (Lourakis et al., 2009).
It starts the reconstruction process using a single pair of images, the so called “initial pair”, this pair should contain many matches and a vastly different perspective. This is essential to avoid finding local minima on large scale SfM problems. Outlier tracks with erroneous keypoints are removed after every run of bundle adjustment optimization. The process then adds pictures (camera poses) and repeats its cycle until no more numbers of 3D points can be added to the model.
On an important side note: the reconstruction of this cloud does not contain real coordinates, for the calculations an arbitrary coordinate system get created. Therefore it is important to have ground control points (GCPs) installed Carrivick et al., 2016).

2.2.3. Production of the dense point cloud, Clustering views for Multi View Stereo (CMVS)

The result of the sparse point cloud is usually only an intermediary step to generate a point cloud which gets used to gather data. For this purpose a dense point cloud has to be generated, that shows an increase in point density of at least two orders of magnitude (Carrivick et al., 2016).
For SfM projects with huge amounts of images another (additional) step can be made. For this the software CMVS (written by Furukawa) takes the sparse cloud generated by SfM and

splits the images into smaller clusters of a more manageable size, (Furukawa et al., 2010). This allows reducing the computing time of the entire cloud (Fig. 11). At the end of the process the different image patches can be remerged together (for example by using CloudCompare) to get the full point cloud.

The computing of the dense point cloud was done using the software Patch-based Multi-view Stereo Software (PMVS), developed by Yasutaka Furukawa and Jean Ponce.
In the first step for each image, blob and corner features are detected and matched across multiple images (Furukawa et al., 2010).

Second step is the expansion of patches; for this neighbouring pixels in the image are used for reconstruction. While excluding discontinuities in depth or already reconstructed neighbouring cells.

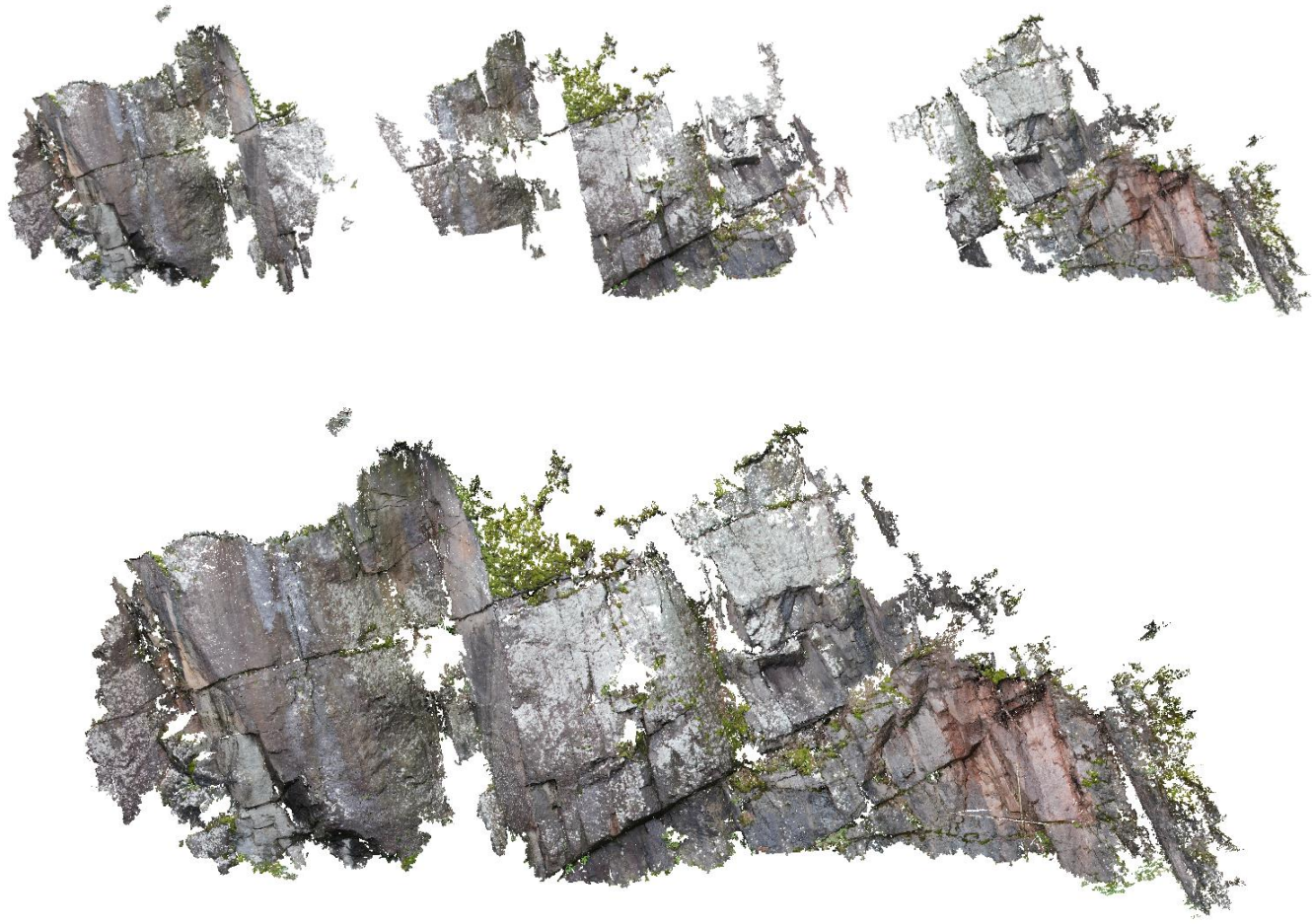

Figure 11: Example of the clustered point cloud of Windlahn, on top the single outputs generated by the SfM-CMVS workflow creating the whole point cloud on bottom, merged with Cloud Compare. Since this dense point cloud was relatively small (8 million points) only three smaller clusters were created.

At last the mismatches and outliers get filtered. For a better result the expansion and filtering process get repeated several times (Carrivick et al., 2016).

2.3. Georeferencing using SfM_georef

The scaling and geo-referencing of the created SfM-MVS models can be done by identifying the ground control points inside the point cloud. Since that is a difficult task, a Matlab software developed by James and Robson 2012 can be used. This is done by using the data from the SfM output. The 3D SfM coordinates are used to derive the transformation to the system of the control data (see Fig. 12 and Fig. 13).

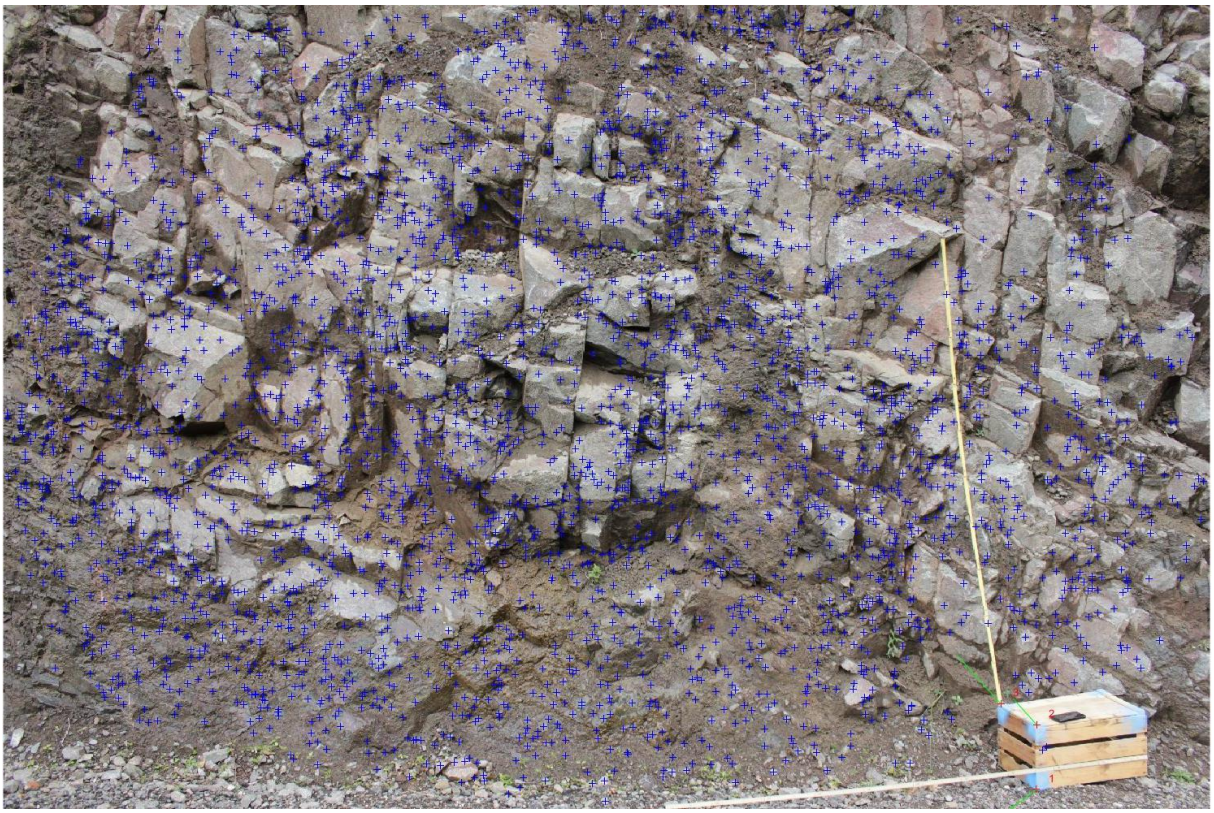

Figure 12: The blue point represent SfM features recognized by the SfM georef program, those are used to transform the point cloud

The necessary data for geo-referencing have to be either 3 or more ground control points (Fig.13) with known coordinates, for simple scaling a single distance would be sufficient.

Figure 13: Example of Ground control points matching, using SfM_georef. The red crosses are the manually selected GCPs inside the picture; the blue circles indicate the position of the GCPs after the transformation; the green lines indicate the shift of each control point.

2.4. Field data Collection

The field survey for each outcrop was made in a short time, using less than an hour for each outcrop while taking around 200 pictures. The chosen outcrops have lengths of about 10-25m with varying heights of 3m to 8m.

To speed up the later referencing and for a quicker field work, a wooden box was prepared. The box had known side lengths and the corners were coloured in blue (Fig. 15, Fig. 16). As a first step the box was placed next to the outcrop and then, using the free app geoClino Free v1.20 (Fig. 15), the dip and dip direction were measured, on a map the coordinates were noted (Fig. 16). With this information it is possible to later reference the gathered data.

Figure 15: Measurement of the Orientation using the app geoClino

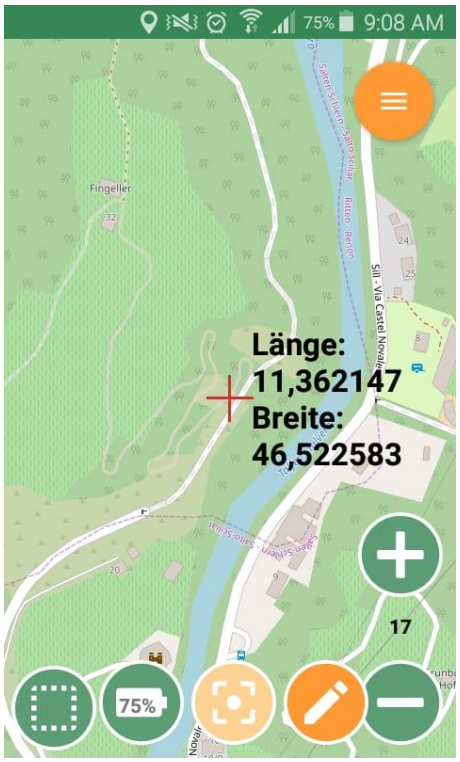

Figure 14: Screenshot of the noted GPS information for the outcrop Alte Sarnerstrasse 1, using the free app Geopaparazzi ©

The actual survey was made in different approaches. For all surveys the overlay between the pictures should be at least 80%, depending on the area of the outcrop, for the edges this value might go down by a bit. Situationally the integrated zoom of the objective was used, mainly to get a better image of the reference box, for the later geo referencing process. Different methods of positioning for taking the pictures where chosen.

For the first approach the pictures were taken sidestep by sidestep, beginning at a close distance of 2 -3 m away from the outcrop at a perpendicular angle to the surface, then moving sideways stepwise (around 1m) for the entire outcrop. After that a second row of pictures closer to the surface was made, at 1m distance with greater angle to catch more of the outcrop, see Fig. 29.

The second approach was to choose a standing point and take pictures of the entire outcrop from that point of view. This was repeated for multiple standing points, taking roughly 20 pictures of each point, or as many was needed to cover the entire outcrop. The points were chosen at different distances, between 1 m to 3 m and varying angles towards the outcrop.

Most of the outcrops were lacking elevated areas around, therefore all pictures were taken

Figure 16: Left; Measurements of the dimensions of the box
Right; Positioning of the box at the outcrop Alte Sarnerstrasse 2

from the same height, if there was a possibility, for example Alte Sarnerstraße 2 (Fig. 35) pictures were also taken from another angle, producing a denser point cloud on surfaces, that otherwise would be in the camera shadow.

2.5. Camera parameters

The camera used is a customary handheld digital single-lens reflex camera from Canon. The model is the EOS 550D, using the EFS 18-55 mm lens. All the images were taken with a resolution of 18 Megapixels; all the adjustable settings were kept as similar as possible for each outcrop on its own. The shutter speed was set at around 1/500 sec; the aperture was set between f/4 and f/5.6, and the ISO speed between 400 and 800.
This was done to receive very consistent images of each outcrop, even though Snavely (2008) proved the workflow being able to work with highly variable pictures for the processing it works better if the images have similar lighting conditions.

2.6. Processing surface cloud and its geo referencing

The processing after the field work is a crucial part of this work, since photogrammetry is a passive remote sensing method; this takes a few more steps. A passive method does not send own signals and measures them, unlike the active method. But rather it uses already existing signals, in the case of photogrammetry the signals are lightwaves (reflected sunlight), and detects them.
A big difference between active remote sensing methods like LiDAR (light detection and ranging) and photogrammetry is, that active sensing has the possibility of using multiple pules of waves to get some penetration of the surface, for example the foliage of trees. Passive remote sensing has is a lot more limited in that regard, to avoid missing points caused by this phenomena it is considered to use multiple different angles and try to remove vegetation covering interesting parts of the outcrops during the field work.
First step for the processing of the gathered data, the open source software “visual structure from motion” Wu, (2013) was used to create a sparse point cloud. For the processing of the dense cloud Patch-based Multi-view Stereo Software PMVS - Version 2, (Furkukawa et al., 2010) was used. This takes the output data from the SfM and then splits the input data into a set of image clusters of manageable size. This results in a dense cloud with different “sub”-clouds that get re-merged together later on.
The process of geo-referencing is essential to prepare the gathered data for further investigative steps. During this each point of the point cloud gets transformed from an arbitrary coordinate system, into a common coordinate system (see Fig. 17). For example the Universal Transverse Mercator UTM32N, this is the system widely used by professionals and the government in this area.
To make this process easier it’s possible to simply rotate and scale the point cloud, leaving the translation for a future step. This means the point cloud get transformed from an arbitrary

coordinate system to the UTM system, with a known (but still shifted) coordinate origin. For example, the outcrop Windlahn is located at UTM32N (682.854,76/5.164.302,7) but for the calculations this point was set to (0/0). This way the values for the coordinates stay small, but with a simple transition (see formula Fig. 18) of the cloud all points would have the real UTM coordinates. This is an advantage since for the purpose of gathering data from the clouds surface the real coordinates are not necessary, only the orientation and scaling have to be correct.

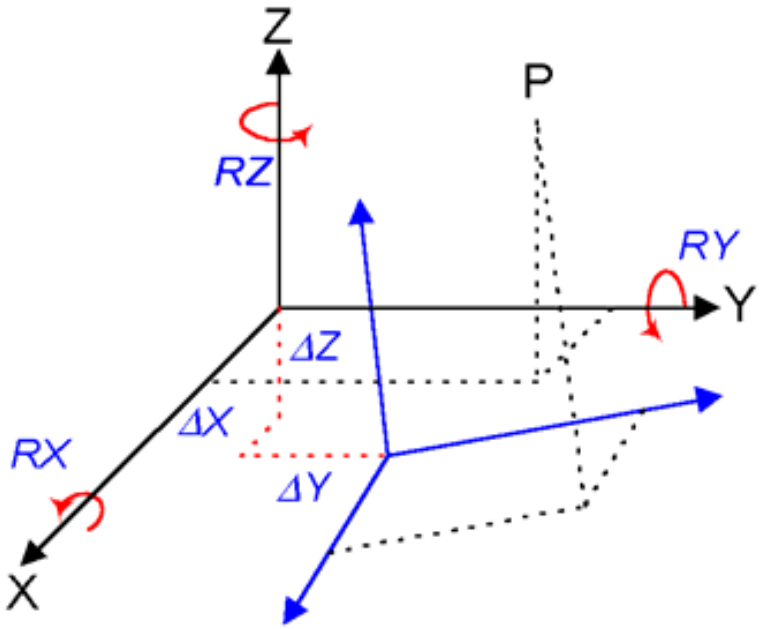

Figure 17: A sketch for coordinate transformation, the whole system get rotated and translated along all 3 axes. For the case of the orientation of the box only 2 rotations were needed, needed, since it was put in horizontally to simplify this work step.
From González et al. (2003)

Going on the next step was to scale and orientate the point cloud; this was done using “sfm georef” created by Mike James, Lancaster University. This tool allows picking targets (points of reference) from the photographs and assigning them coordinates. For this study the targets were the corners of the box.
Beforehand the real coordinates of at least 3 corners of this box were calculated using a simple coordinate transformation matrix (Fig. 18) calculated with LibreOffice calc. This was necessary, because all the information gathered in the field was the orientation and the dimensions of the box; reason being to try to simulate a fast, low budget field investigation.

To test out the software, different amounts of reference points were chosen. With just 3 ground control points the software already shows an accurate result, presenting a good match on the photos of all coordinates, even in pictures that were not picked to reference the point cloud afterwards.

$$R_x(P) = \begin{bmatrix} 1 & 0 & 0 \\ 0 & cos\,\Phi & -sin\,\Phi \\ 0 & sin\,\Phi & cos\,\Phi \end{bmatrix}$$

$$R_y(P) = \begin{bmatrix} cos\,\Theta & 0 & sin\,\Theta \\ 0 & 1 & 0 \\ -sin\,\Theta & 0 & cos\,\Theta \end{bmatrix}$$

$$R_z(P) = \begin{bmatrix} cos\,\Psi & -sin\,\Psi & 0 \\ sin\,\Psi & cos\,\Psi & 0 \\ 0 & 0 & 1 \end{bmatrix}$$

Figure 18: Transformation matrix used to generate the UTM coordinates using the in-situ measurements for Θ = dip and Ψ = dip direction. The transformation of the X axis can be avoided, since the measurement of dip and dip direction always are made relative to a horizontal line.

The only difficulties using this tool appeared if there were just a few pictures from a few angles of the box. On the users end it is also important to get a good angle toward the ground control points, for example try to avoid shallow angles towards the target points.

2.7. Digital extraction discontinuity characteristics

The rock surface information was generated by the program CloudCompare. The normal vector for each point of the cloud was created using the add-in “hough-normals”. The basis for this calculation step is written by Boulch et al. (2012).

In the following steps the cloud is saved as a .txt file to create a point cloud that’s widely accessible with different programs. During this step data about the information about the colouring (RGB) was eliminated. The result is a point cloud with the basic information for XYZ and additionally the corresponding normal vector for each point.

Now with the information about the normals of each point, the program CloudCompare allows to show the varying information using a scalar field. First a colour scale was created, plotting a different colour at every change of 5 degrees angle in dip-direction (Fig. 25). This way the visual scalar field gets a more intuitive colour-code, so the discontinuities with similar dip directions will have the same or at least very similar colours. With this step done it is possible to distinguish visually the different sets inside the outcrops. Each set gets limited to reasonable values, around a variation of 30° in dip direction and around 20° in dip, and then

exported as a new cloud. This was repeated for all distinguishable sets of the outcrops. By doing this the outcrops information gets broken down to these sets, reducing the overall data. At the same time this step is essential to get rid of points that do not represent geological features, for example vegetation.

As a control is good at this point to compare the surfaces of the extracted sets and the entire surface, allowing seeing if there are any important surfaces missing (for example Fig. 46).

With the sets extracted from the cloud, the gathering of information of the set begins. Using the compass plug-in of CloudCompare, the orientation of the set was measured on different surfaces of the set (Fig. 11), multiple times to get a reasonable amount of values. The orientations were measured by using the orientation tool, by rotating the cloud and pick all obvious surfaces of the same set. These measurements were later on plotted using Openstereo (Grohman et al., 2010) to create stereographic plots of the discontinuity sets. For this step other, freely available programs would also be possible to use, for example Stereonet 10 by Allmendinger et al. (2012). Such results are crucial when it comes to describe rock mass behaviour and possible failure mechanisms.

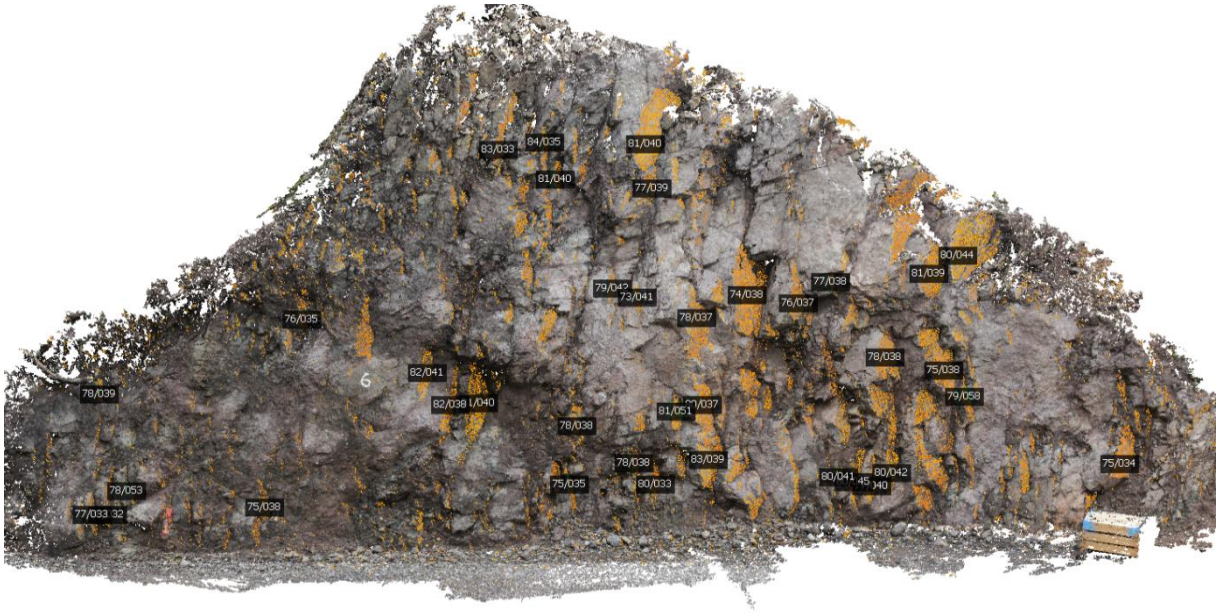

Figure 19: Measurements of the orientation of the discontinuities using the CloudCompare Compass tool (example from Alte Sarnerstrasse 2)

Different approaches were tried to get semi-automated results for the spacing of the discontinuities. For all approaches the spacing was first measured by using the compass tool of CloudCompare: of one-point-thickness (Fig. 21). For this procedure a typical large surface of a set was picked and from there the distances to all the visible joints were measured. All of this data was exported to a XML-file, and the repeated for each outcrop and each set.

The idea behind the one-point-thickness approach is to get all the possible distances between the joints of a set, afterwards the difference between the distances were calculated to give an indication of the actual spacing between the joints of a given set.
Using LibreOffice Calc., the measured distances were sorted by length, and then the distance difference between the two closest joints was calculated. For simplification, on the first approaches only differences bigger than 10cm were considered to act as distinct joints, just because of the possible deviations of the distance measurements. These deviations are due to the way the plug-in works, the one-point-thickness gets measured from a single surface. This surface therefore has to be representative for the entire discontinuity set, so if this picked surface now has a slight angle to the mean orientation of the sets all the perpendicular measured distances are slightly tilted.

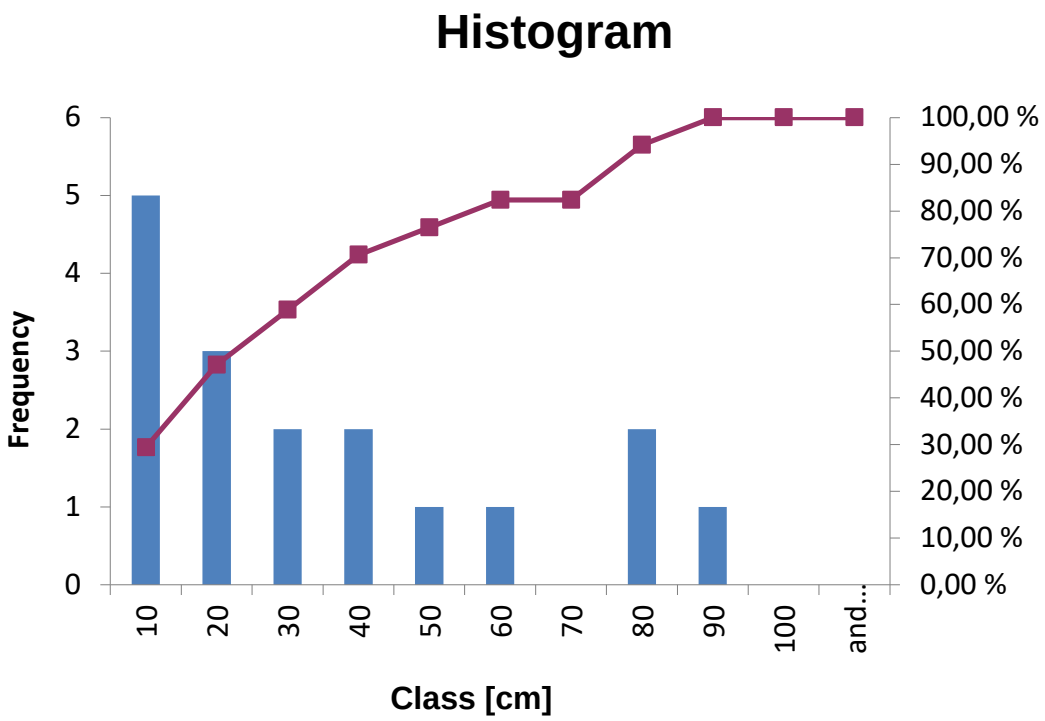

Figure 20: An example of the second approach to create a histogram of the measured one-point-thickness. Clearly visible is the peak at the 10 cm class. Not showing any other peaks that would clearly define other sets.

The problem using that approach is, that the calculations are only give a rough indication of the spacing, since the spacing gets only calculated between the distance of two measurements. If those measurements for example hit the same joint at different surfaces a slight change in distance, a few cm, is most likely. This would create way too many fake joints by taking lots of measurements. To get rid of this problem a 10 cm “safety-window” was introduced to the approach, by summarizing measurements to one set that had less than 10 cm distance in between them. This idea did not solve the original problem, since now with a lot of measurement that were closely together, they appeared as one set. For

example: would there be 4 measurements that are all 9 cm apart using this approach it would consider them as the same joint, even though they are in reality 27 cm apart and therefore could be defined as different, distinct joints.

As an alternative approach the spacing between the obvious joint surfaces was measured in CloudCompare, and with no further exclusion a histogram with class steps of 10 cm was generated (see Fig. 20). This way no data gets lost. But this idea also shows a big flaw, the data selection using CloudCompare has to be done very carefully, to not lose out different joints. Also the observation bias has a big influence since the histogram was plotted only with the amount of visible joint surfaces.

The third idea for estimating the joint spacing between the joints of the same set is to calculate the mean orientation of the set, using the gathered data from the dip and dip-direction. Using this value then creating a single plane inside CloudCompare and measure all obvious joint-surfaces to this base-line-plane.

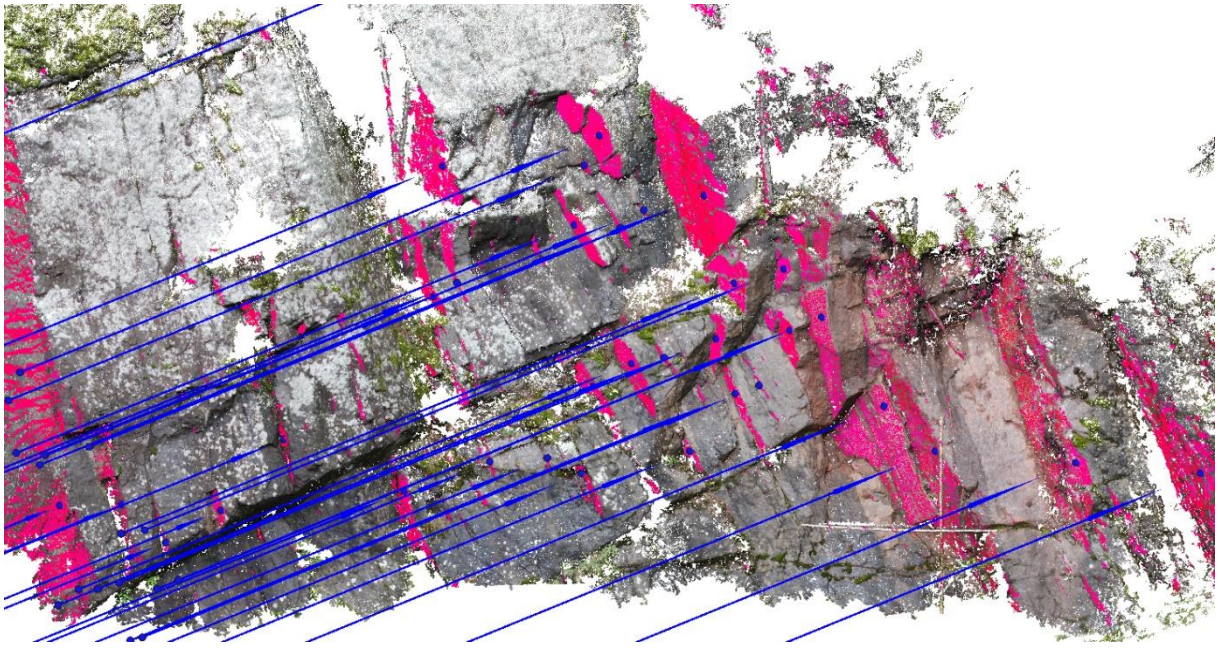

Figure 21: Example of extracting the discontinuity characteristics from the point cloud, the orientation was measured on the surfaces; meanwhile the normal distance got measured from a starting surface to each point of the other surfaces those surfaces

In the end it was decided to use the third approach by measuring the spacing directly from the point cloud by picking the most persistent surfaces. Starting from them, the normal distances to the other set-surfaces got measured, if the distance was multiplied between the surfaces; they were defined as the set spacing. This approach is time consuming, but avoids errors of a semi-automated extraction of the spacing. Nevertheless it only worked for the more “natural” outcrops; the freshly excavated outcrops had a very small spacing due to the recent mechanical abrasion.

3. Results

The results of the workflow were dense point clouds for all of the outcrops, which were used to digitally measure different rock describing parameters. From a structural point of view a detailed description of the discontinuities is very important (see chapter 2.1), therefore for all outcrops the dip and dip direction for all the different discontinuity sets were measured and so was the spacing. As a further step the orientation was plotted in pole point diagrams, to be able to compare the results and get further information about the accuracy of the orientation measurements. Other Parameters like roughness and termination could not be directly measured using the SfM tools on the scale of outcrops with 10s of meters; this would be only possible on close-up settings with less than 1 m.

3.1. Outcrop: Windlahn

The outcrop is located at the road leading to the hamlet of Windlahn (Fig. 22). Unfortunately the CARG (Geological CARtography) project, creating geological and geothematic sheets on a scale of 1:50.000 covering the entire national area of Italy does not cover the area of the outcrop. But using the information from the geological map (ISPRA, 1:100000) the area is defined as porphyric quartz (Rhyolite) and therefore it is part of the Athesian volcanic group. This information can be confirmed by the field observations. The surface itself was most likely profiled by humans during the construction works for the road; nevertheless the main

Figure 22: Orthphoto of the outcrop location along the access road to Windlahn, on the left of the picture (in yellow) is the national road S.S.508.

parts stayed most likely untouched, due to the large block size caused by the joints. The size of the outcrop is about 22m wide and 8m height (Fig. 23).

The most interesting point of this outcrop is that there are very persistent and far spaced discontinuities. This outcrop is a great testing site for the process of data extraction from the rock surface.

The weather during the photo-shooting was cloudy, but it had rained the day before, and therefore the surface was wet in parts. In addition to that, sparse vegetation was covering parts of the surface, creating some sparse areas in the point cloud (Fig. 24). The pictures were taken sidestep-wise, with a distance of roughly 2 m to the outcrop surface (Fig. 26). At each step three or more pictures were taken in vertical direction, this was done straight, to the left and to the right. In the end some oblique pictures were taken as well, to get a better angle on some surfaces. In total for this outcrop 174 pictures were used to create a point cloud with around 6,7 mio points. (Fig 24)

Figure 23: Panorama photo of the outcrop, the angles are distorted due to the panorama-projection.

Figure 24: Dense point cloud of the outcrop, the white patches is areas where vegetation covers the rock surface. On the bottom right a fresh breakout is clearly visible (reddish colour) that also follows the same joints as the other surfaces

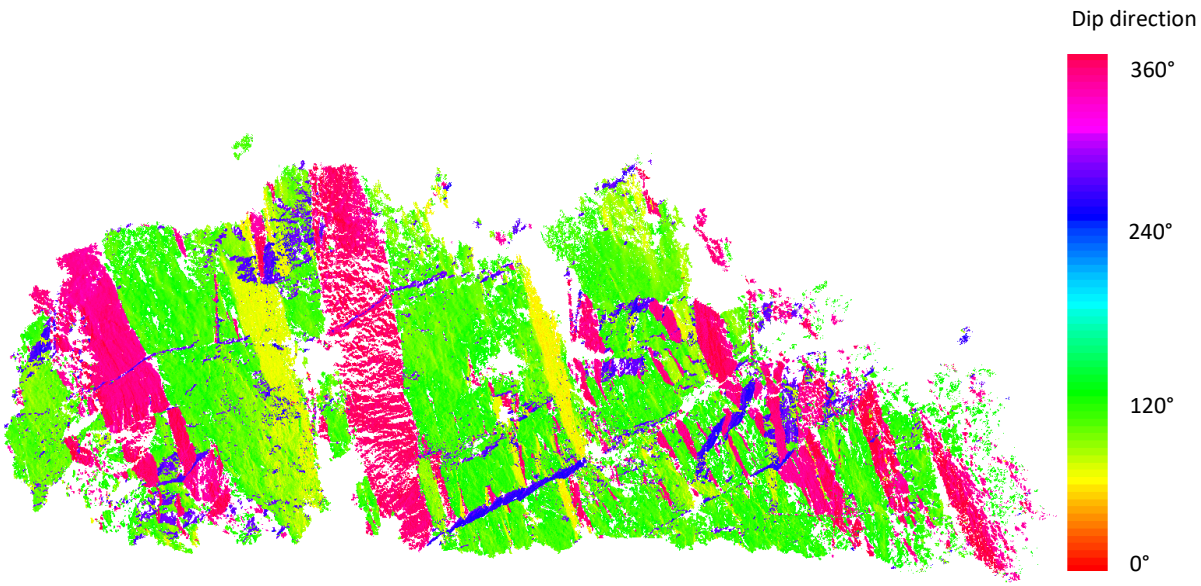

Figure 25: The four sets resulting with the CloudCompare analysis

Set 1 = green

Set 2= blue

Set 3 = magenta

Set 4 = yellow

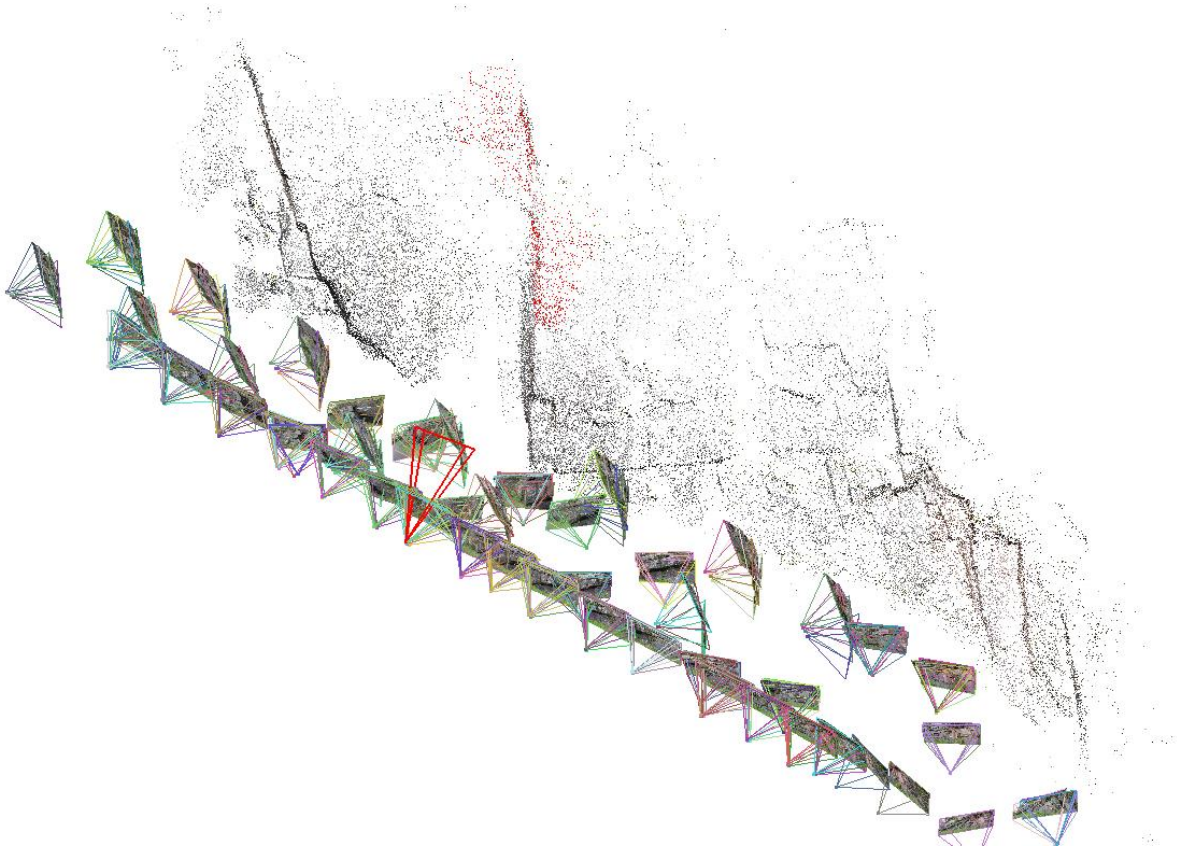

Figure 26: Camera positions for Windlahn

The analysis to define the sets using CloudCompare for this outcrop was rather simple, due to the very distinct and persistent joint forming the surface, the few patches of vegetation also didn't influence the results. As shown in Fig. 25 there are four very prominent sets, 3 vertical/sub vertical ones and one. The stereonet (Fig. 17) shows the results well, the set 2 (blue) shows a bigger variation in the plot, this is due to lacking surface areas, caused by the observational bias.

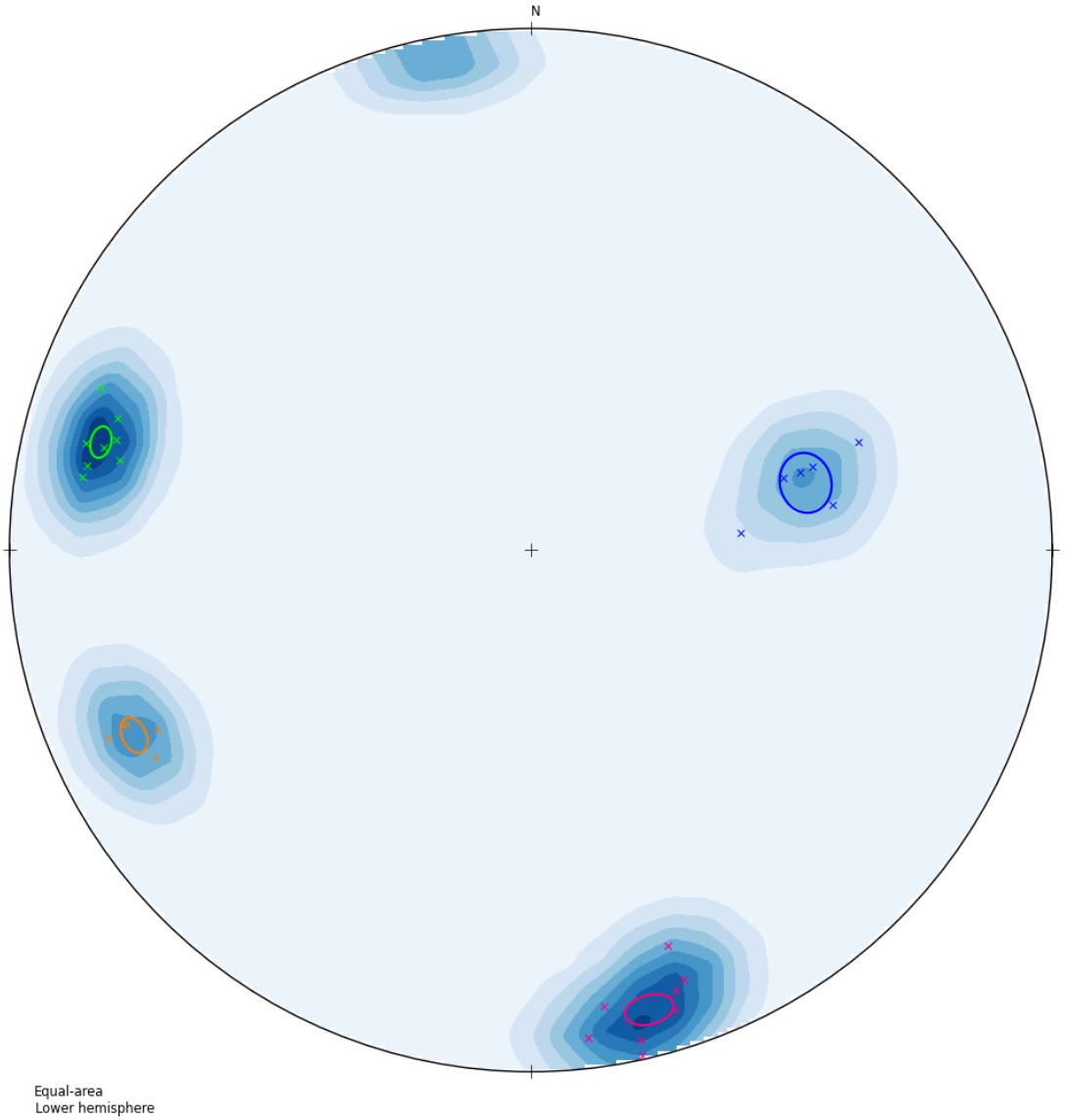

Figure 27: Stereonet-plot of the measured set-orientations. With the 95% confidence cone

Set 1: green

Set 2: blue

Set 3: magenta

Set 4: orange

After the investigations of the point cloud as a whole and the polepoint-plot (Fig. 26) it is possible to state, that the vertical joints most likely formed during the cooling process of the rock and therefore they are very persistent. Meanwhile the shallow inclining joint might have formed as a pseudo-bedding plane to release the stresses acting vertically.
The polepoint-plot also shows that the subvertical sets 1,3 and 4 have a much smaller cone of confidence and therefore the measured values are much tighter together.
At Fig 27 the contour lines close to the North are part of the set 3, this happens statistically since the discontinuities are almost vertical, they could also show a dip direction with an additional 180°, but they still remain the same set.

The parameters of the rock structure of each set will be presented in Chapter 3.6

3.2. Outcrop Halbweg

This outcrop is located in the middle of the Sarntal gorge, next to the national road Sarntaler- und Pfitscherjochstrasse (S.S.508) at kilometre 9.3 (Fig. 28). It used to be the old access road for the valley. From a geological point of view the outcrop is formed by Ignimbrites of the Athesian volcanic group. (CARG sheet 27, Bolzano)

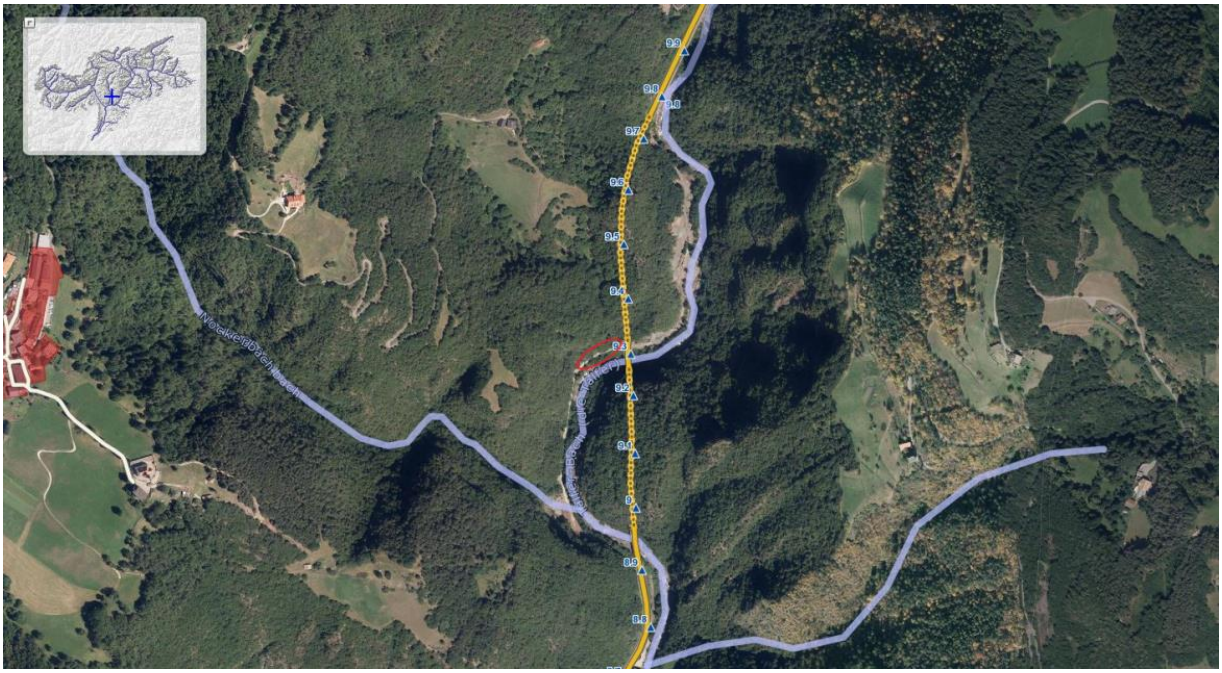

Figure 28: Location of the Outcrop Halbweg, accessible via the main road S.S.508, next to the river Talfer

The outcrop lies insiede the Sarntal gore, and is defined by vertical rock walls (Fig. 29), with very persistent discontinuities. The rock surface is only slightly altered; this is due to the fact, that during the lifetime of the old access road the walls were kept in good condition to prevent rocks falling on the street. Despite the unfavourable dip direction of the discontinuities (see Fig. 5) the rhyodacitic walls were stable and held up without further safety measurements. During the field work only a few individual blocks, which had fallen from above, were found along the road

For this site 258 pictures were shot, from 11 different positions (Fig. 30), doing approximately a 180° view in front of the outcrop. This resulted in a roughly 20m wide and 10m high model of the outcrop (Fig. 32).

Figure 29: Overview of the outcrop. The picture is taken parallel to the subvertical discontinuities of the set 1, showing well their orientation and persistence through the rock mass.

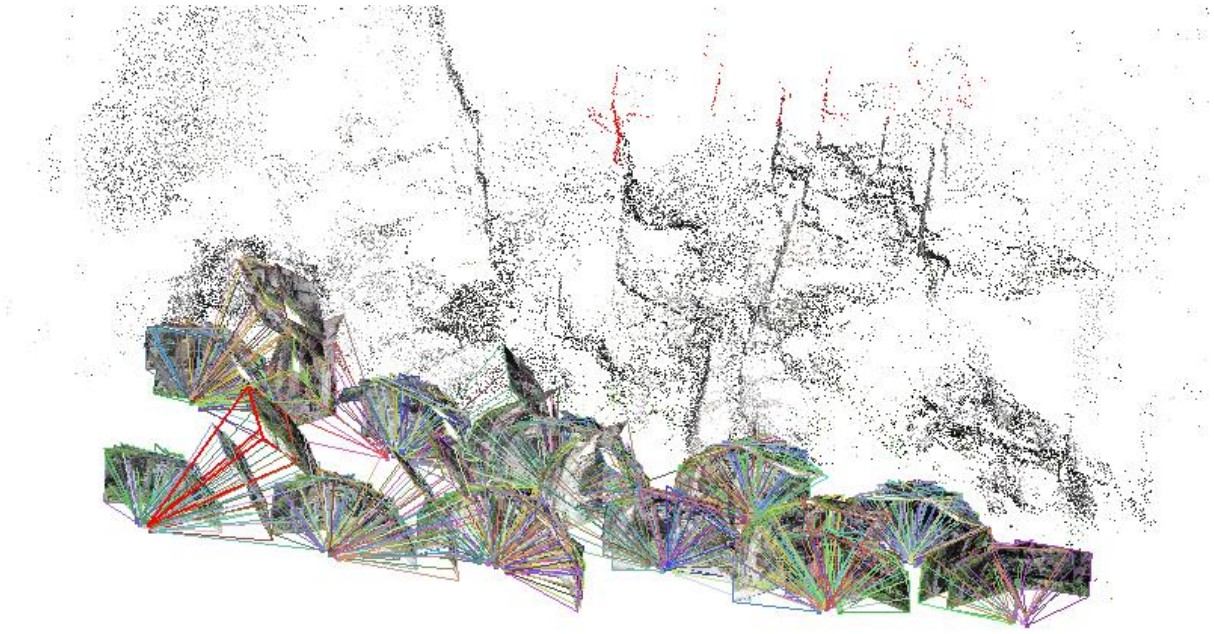

Figure 30: Positions of the pictures taken, the different standing points are each forming big cones.

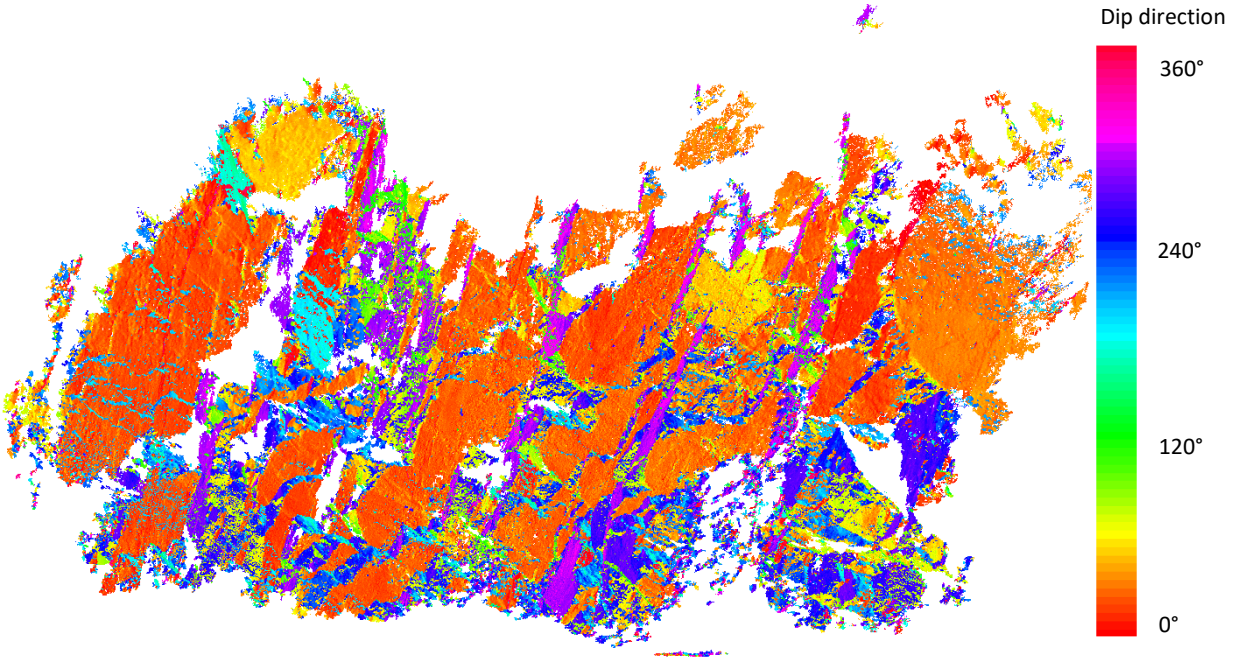

Figure 31: Results of the Hough normal, created a scalar field for dip-direction.

Set 1: orange

Set 2: magenta (purple)

Set 3: green

The blueish surfaces are formed by the erosion of the rock, this also explains the big variation in dipdirection, those were not considered a distinct set.

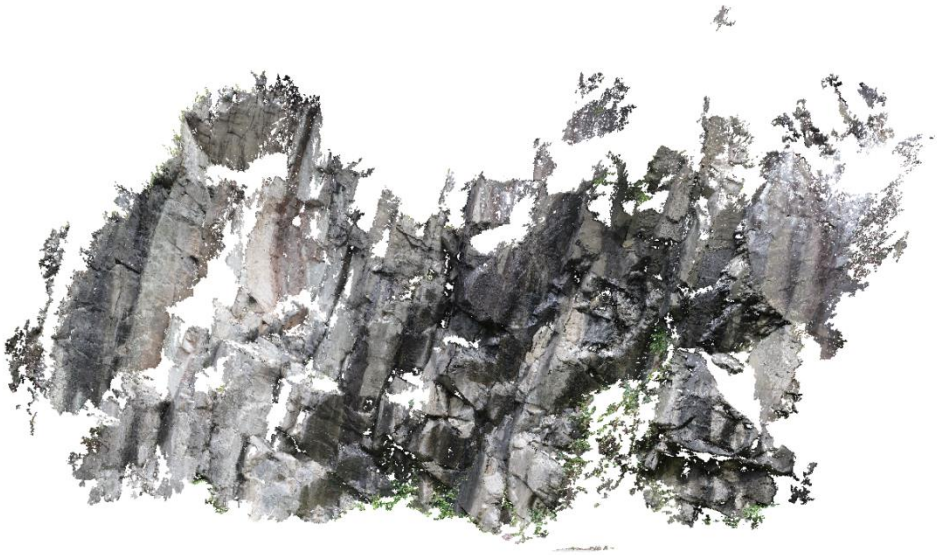

Figure 32: Pointcloud of the outcrop, the areas without information are vegetation (on the bottom right), and caused by the orientation of the surface (left side). Latter could be changed by taking more pictures from an elevated point of view to the left, unfortunately there was no such place.

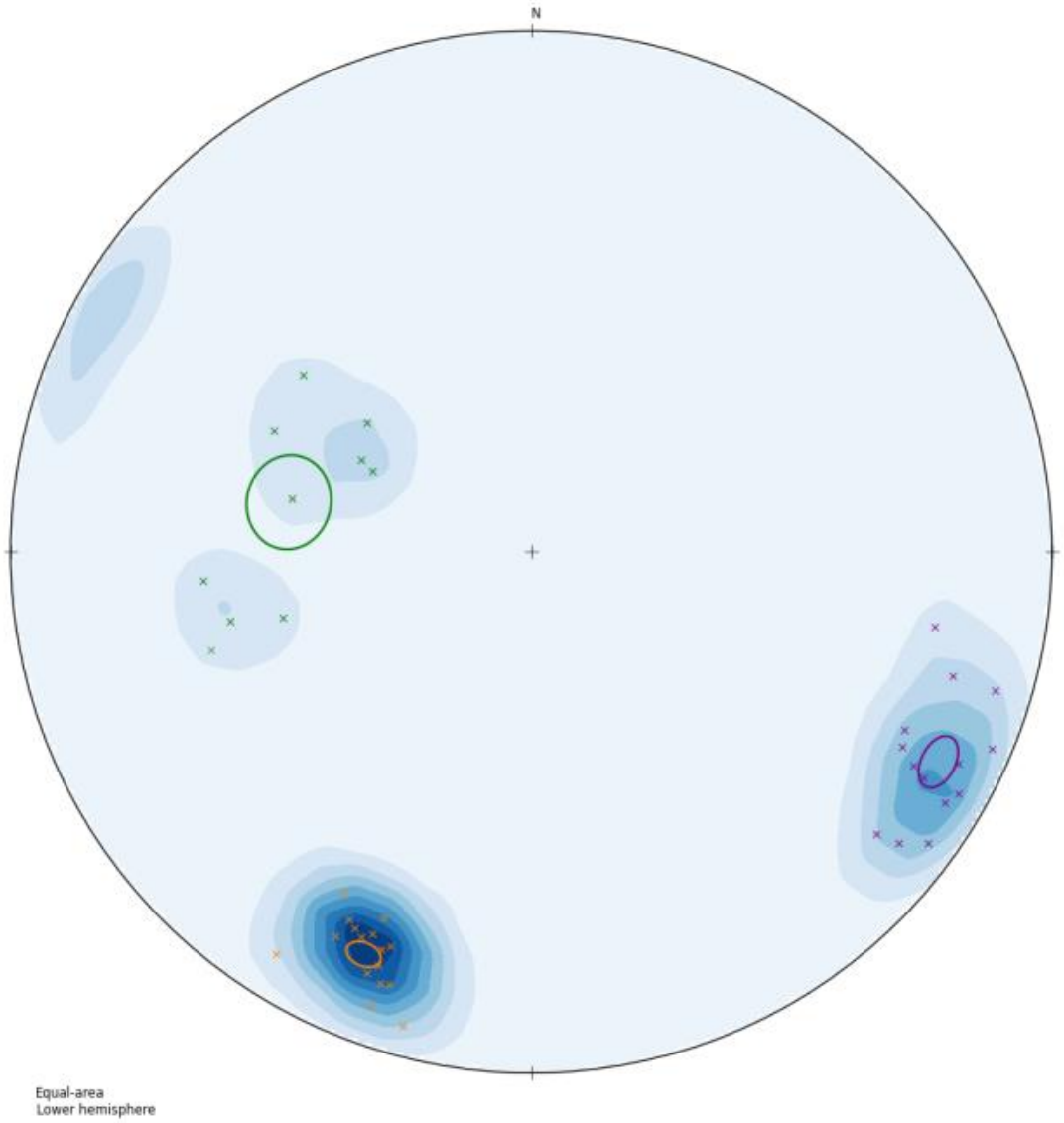

Figure 33: Stereonet of the Outcrop
Set 1 (orange)
Set 2 (purple) showing little variation
Set 3 (green) shows a lot more deviations

The outcrop shows 2 very distinct and also very consistent joint sets, being almost vertical, therefore the origin being cooling cracks that build soon after the eruption. And a 3rd set, that shows an eastward dip direction, with a big variation of the orientation, the origin of this joint-set is most likely the exhumation of the rock or some other brittle tectonic stress. The distinctive sets are already visible in (Fig. 29, Fig. 31), set 1 being the one straight in the picture (orange colour) forming the biggest surface areas of the outcrop. Set 2 is visible with magenta to purple hue, and lastly the set 3 is formed by the joints with the green colour (forming a sort of pseudo-bedding).

The parameters of the rock structure of each set will be presented in Chapter 3.6
The weather conditions were fine, but the day before there was rain, that's why parts of the outcrop still were wet, creating dark patches on the surface (Fig. 34). This did not cause any major problems for the workflow.

Figure 34: Close up of the outcrop, the wet patches are clearly visible on the righter side. But also other parts had changing surface colours

As a further step of investigating the SfM workflow, the repeatability of it was put to the test for this outcrop. To achieve this, the entire processing was repeated, beginning from the creation of the point cloud. The same pictures were used to create a dense point cloud. And then this cloud was transformed again and put to comparison next to the first results. It is important to note, that during the transformation process, some deviations may have occurred, since the ground control points are selected manually. Therefore a small difference between the resulting point clouds has to be expected due to human error.
On a general not the second version (see Fig. 35 bottom) has fewer points in the dense point cloud, in numbers around 10,3 mill. versus the first iteration having around 12,4 mill. points.
A possible explanation of this is found when looking at the step of the creation of the dense point cloud (see Chapter 2.2.3). The image input was exactly the same but during the process the program split the information in different ways, this can be seen when comparing the clusters generated for the same data (see Fig 36).

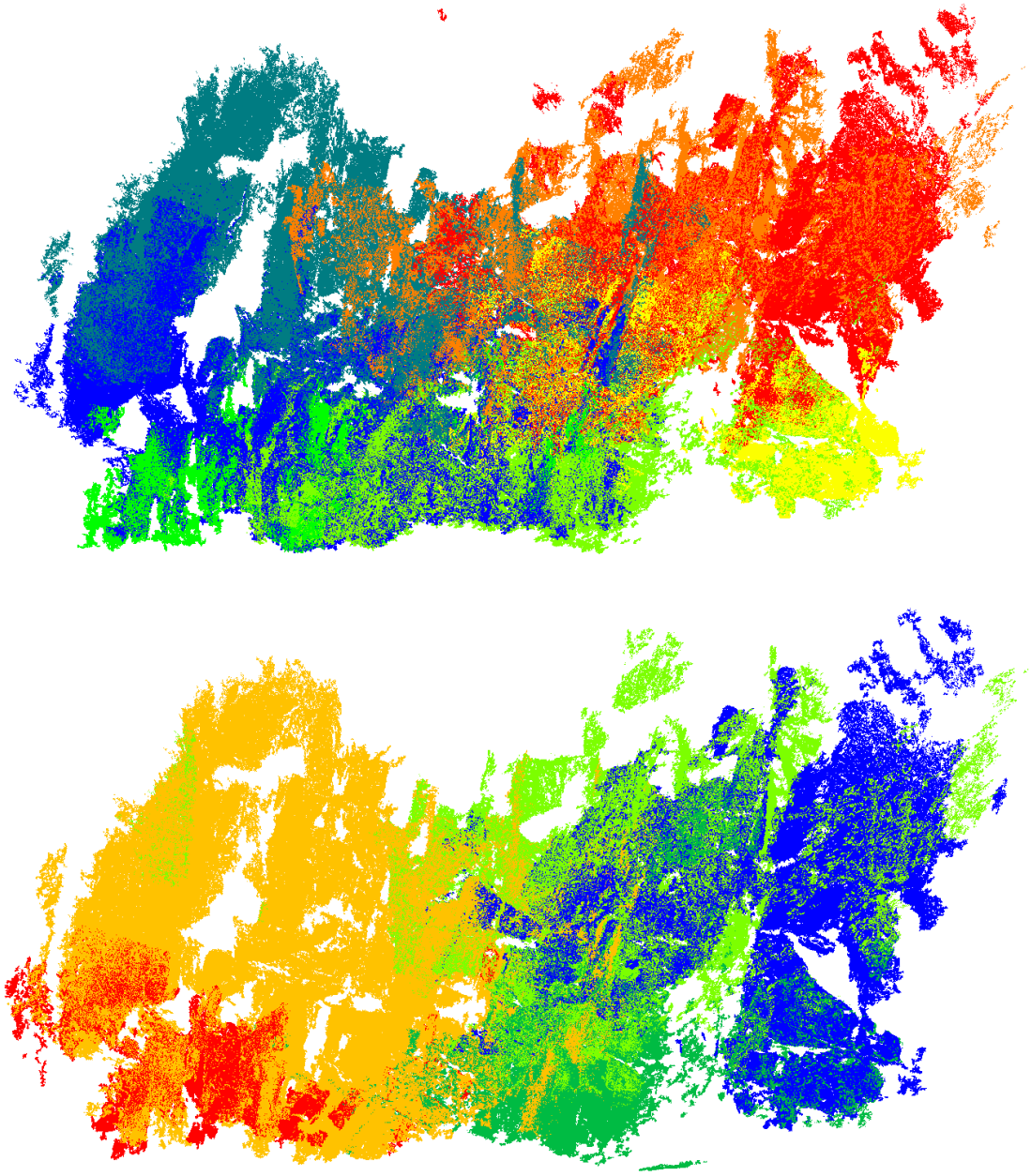

Figure 35: Comparison of the two separately generated point clouds for the outcrop Halbweg. The colour of the scalar field simply represents the different clusters created during the creation of the dense point cloud. On top there is the first iteration with 6 “sub-clouds” merged together, on bottom the second version with only 4 “sub-clouds” creating the full, dense point cloud.

This drop in points is only noticeable on a few spots when comparing them directly together, for example on the bottom, where the green patches of vegetation are much denser on the first version (see Fig 35. top).
Overall both clouds are well suited for the purpose of data extraction, even when considering the slightly differences (see transformation matrix Fig. 35)

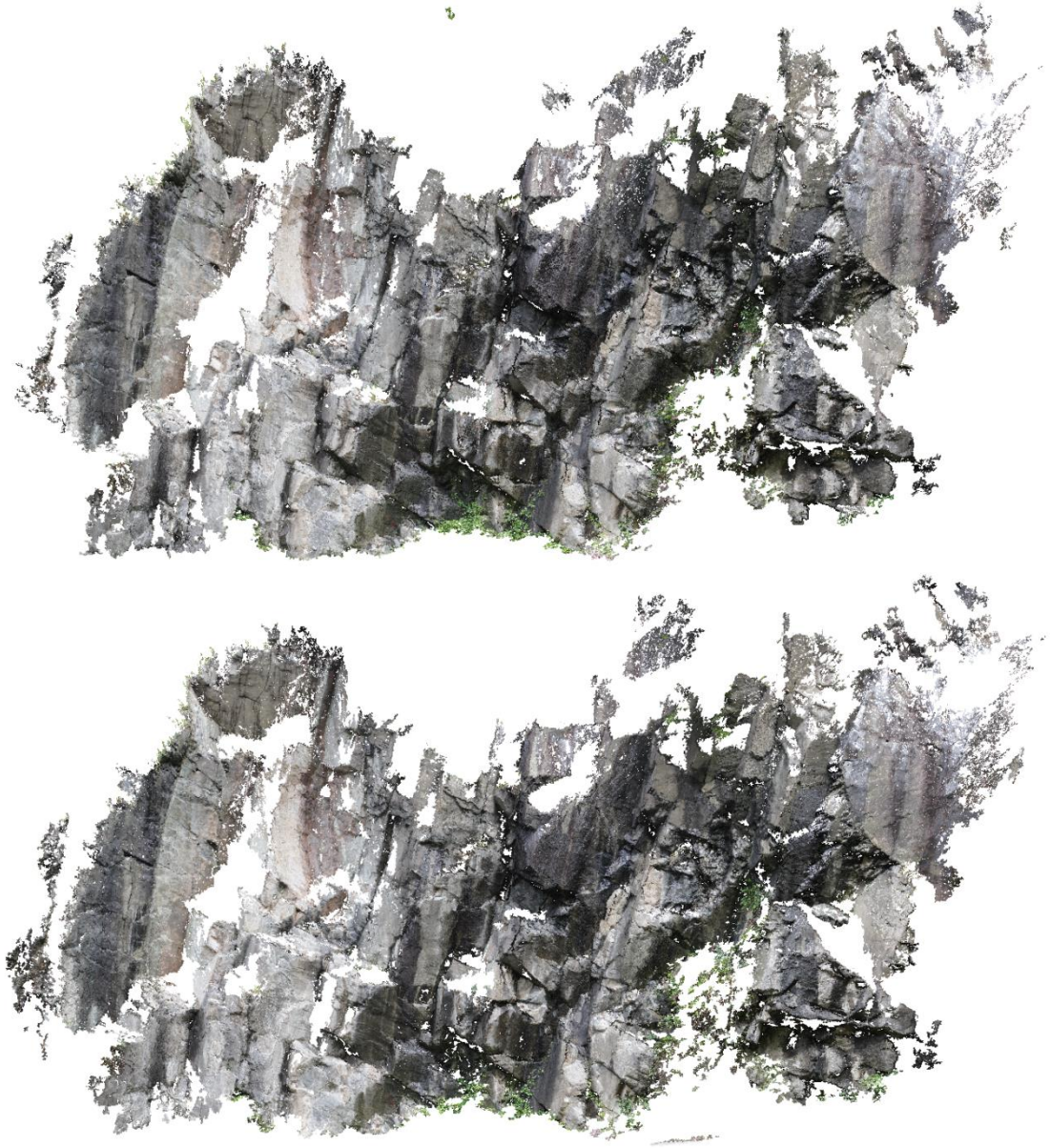

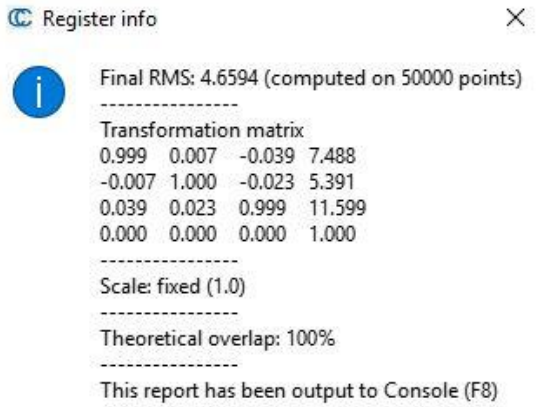

Figure 36: On top is the coloured point cloud of the first calculations, in the middle the point cloud to compare. On the right side the transformation matrix, between the two clouds. The scaling is almost perfectly, with only a small shift in the different axes (last column, values are in cm).

3.3. Outcrop: Alte Sarnerstrasse 1

This outcrop is located in the north of Bozen, along the old road leading into the Sarntal valley until 2016, more specifically between the first and second tunnel, where a new access road for a farm was built in 2018 (Fig. 37). Geologically speaking this outcrop is located inside the Ignimbrites of the Athesian Volcanic group (CARG sheet 27, Bolzano).

The construction of this road resulted in big cuts in the morphology, showing lots of fresh joints of the rock mass. Unfortunately not all of the surfaces are caused by persistent joints penetrating the rock mass, but rather created by the mechanical forces applied by the excavator. This results in many small surfaces (Fig. 38), creating a big bias when it comes to define the spacing of the different sets, but on the other hand allowed many measurements of orientations of the sets.

The dimensions of the investigated section of that outcrop reached a length of roughly 25m and a height of slightly over 8m. For this outcrop 200 pictures were taken, not from a few positions, but rather perpendicular to the surface with a distance of about 2m (Fig. 39), with sidesteps of roughly 1m. At the end due to the possibility of a higher point of view, more pictures were taken from a small elevation on the other side of the road.

This more face-on approach to the outcrop resulted in a dense point cloud with about 13 mill. points.

Figure 37: Orthophoto of the area around the outcrops Alte Sarnerstrasse 1 and Alte Sarnerstrasse 2

An important note on this outcrop is the difference of the fracturing inside this outcrop, at both ends the discontinuities show a very thin spacing (often less than 1 cm) an also the central part, on the right of the drainage duct (see fig 38) is highly fractured. These areas still show a good resolution when it comes to the point cloud, but handling these small areas to gather information using CloudCompare showed to be a rather difficult, and sometimes impossible task.

Figure 38: Top; overview picture of the outcrop, most noticeable is the drainage duct in the middle. Bottom; Detail of a highly fractured zone at the upper edge of the outcrop

The approach to take a lot of face-on pictures seemed to result in a denser cloud than on the other outcrops, it was decided to manually reduce the amount of used pictures and compare the results to the “full” version, to see at where the “golden point” between the quality of the result and the amount of pictures used lies.

To test this pictures got cancelled out progressively; at first only 150 pics were used and then they got further reduced to 100pictures (Fig. 39 and Fig. 40). This resulted in a more and more sparse cloud, while speeding up the calculation time (see chapter 3.5).

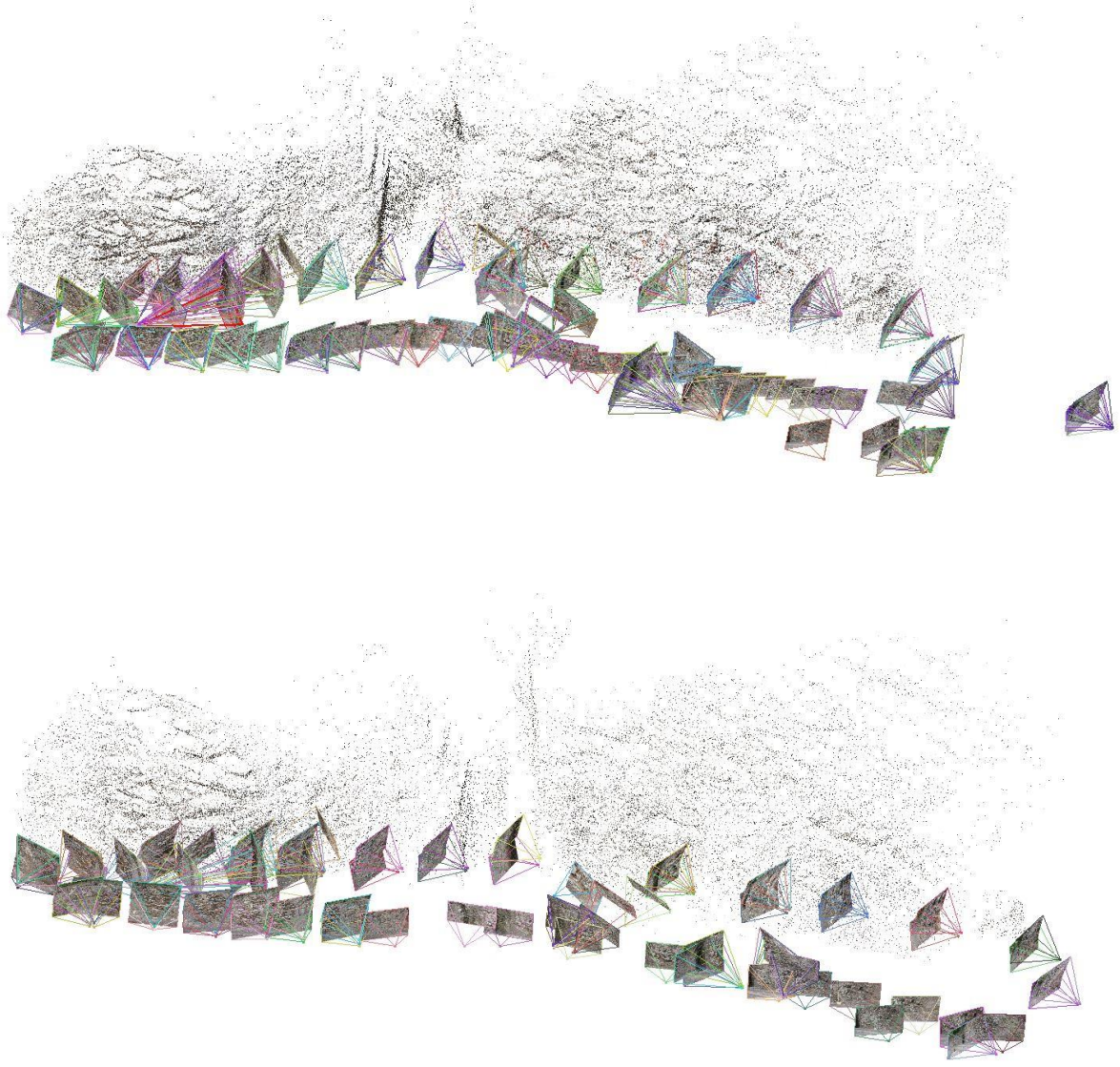

Figure 39: The top figure shows all the camera positions for the Outcrop Alte Sarnerstrasse 1: showing a continuous row of face-on pictures and a closer row of pictures with an oblique angle, trying to capture the point sets perpendicular to the surface.

On the bottom are the reduced camera positions chose to fasten up the creation of the dense point cloud.

The difference is quite visible when looking at Fig. 40 (top vs bottom), especially the density inside the drainage duct is reduced by a significant amount; also the higher elevated areas have a reduced point density. Nevertheless the main features are still well visible. It is also possible to use the smaller cloud to extract the information about the orientation of the sets. The two point clouds also show a very good correlation when it comes to the georeferenced properties, with a theoretical overlap of 100% and no noticeable change in scale (Fig 42)

Figure 40: Top: Results for the approach with all the pictures taken for the Outcrop Alte Sarnerstrasse 1; the cloud shows sparse areas only at the edges and on surfaces orientated upwards (not caught by the camera).
Bottom: Point cloud result, using fewer pictures (camera positions from fig. 28 bottom)

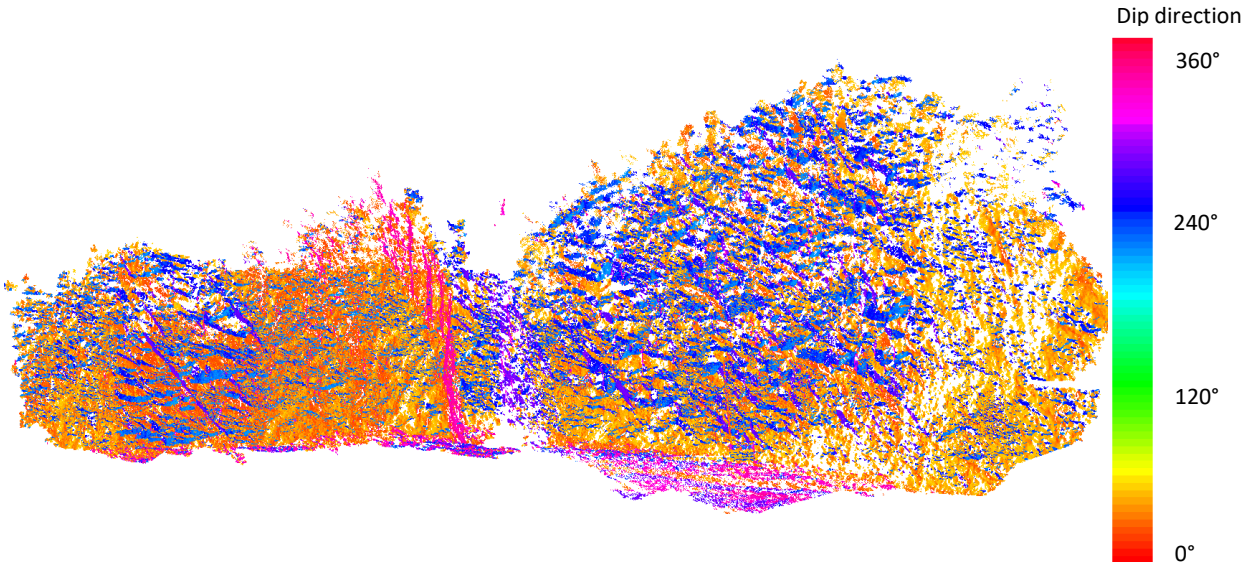

Figure 41: Scalar field of the outcrop, only the data from the chosen sets are plotted. The area on the left of the drainage duct shows clearly a less defined surface. This rough appearance is due to the surface being highly fractured combined with thin spacing

The analysis of the outcrop at first showed 5 sets, but set 3 was later ignored since it could be seen as a part of set 4.

The stereonet (Fig. 43) shows 4 sets, Set 1 and Set 4 are conjugated sets; Set 5 appears only next to the canal. Set 2 is of special interest, since it shows a very strict orientation, good to see on the right side of Fig. 41 where it intersects all other discontinuities.

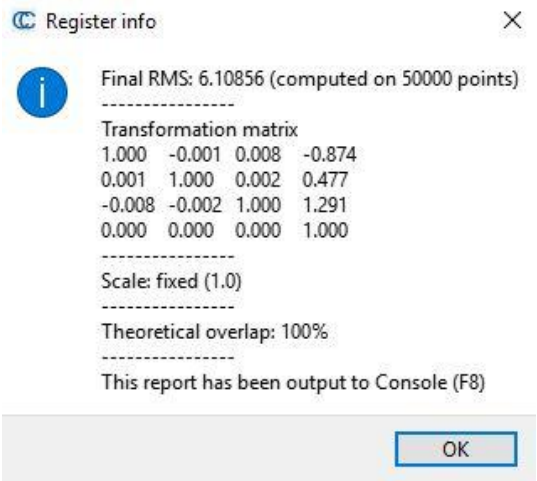

Figure 42: Transformation matrix between the point cloud using all pictures and the point cloud using only 100 pictures

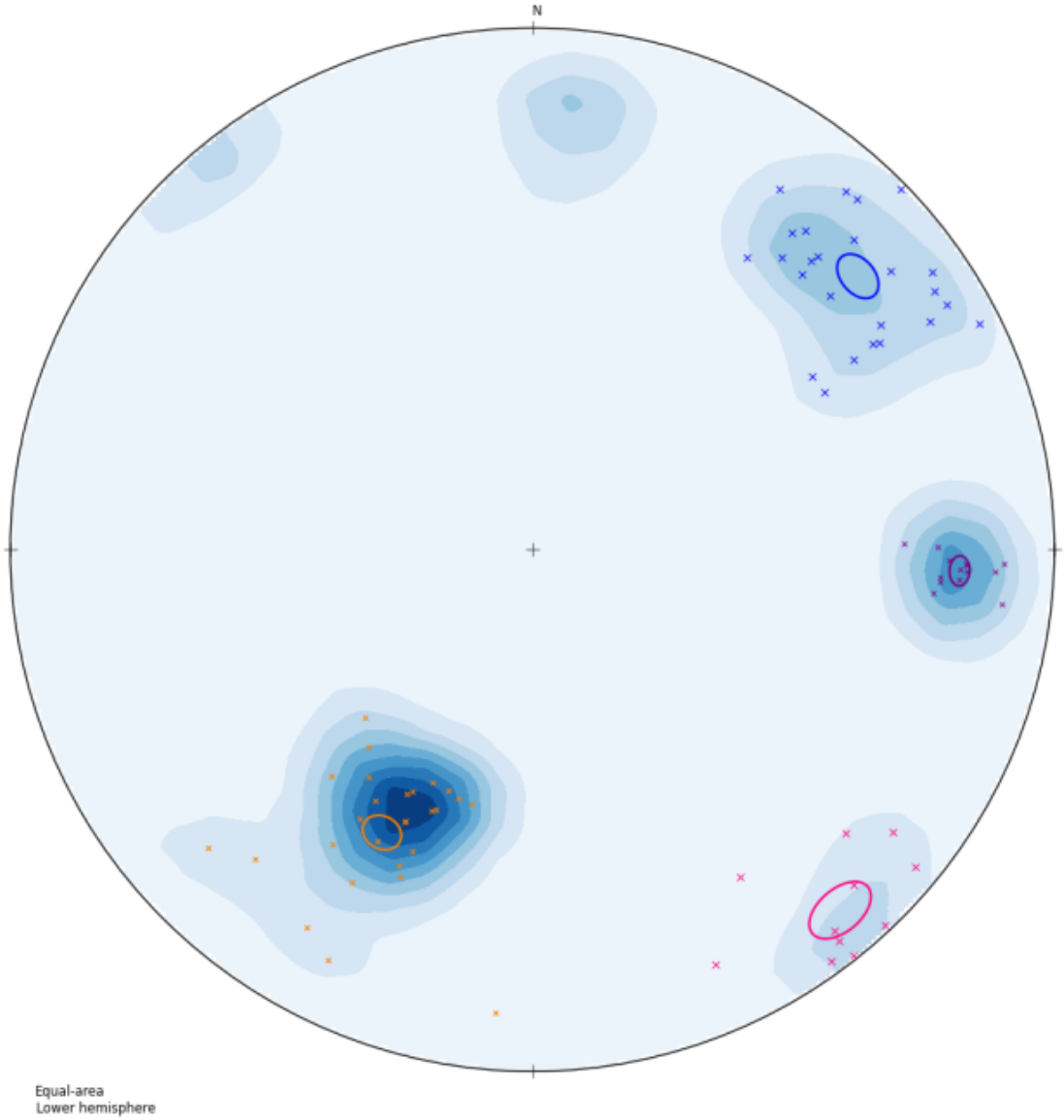

Figure 43: Stereonet for the outcrop Alte Sarnerstrasse 1

Set 1: Orange

Set 2: Purple

Set 4: Blue

Set 5: Magenta

A view on the stereonet shows that, similar to the other outcrops, the main discontinuities show an almost vertical dip. This is ture for set 1 set 4 and set 4, only set 4 is defined by a shallower dip. The circle of confidence for 95% shows a significant variation for the sets 4 and 5. The reason for it being the rougher surfaces of set 4, while set 5 only appears close to the drainage duct and therefore underlies heavily the observation bias. Set 3 (Fig. 41, cyan colour) was dismissed as a set, since it could be split up between Set 2 and Set 4.

The parameters of the rock structure of each set will be presented in Chapter 3.6

3.4. Outcrop: Alte Sarnerstrasse 2

This outcrop is located to the south of Alte Sarnerstrasse 1, a bit higher up the access road leading to the farm (Fig. 37). Due to its proximity to the other outcrop the geology stays the same and it has to be expected to see some similar geomechanical features of the rock mass. The investigated area extends over a length of 10m and a height of 4,50m.
To cover the outcrop 207 pictures were taken, creating a dense point cloud with around 14mio points (Fig. 44).

Figure 44: Point cloud of the outcrop, on the bottom right the box used for geo-referencing is clearly visible

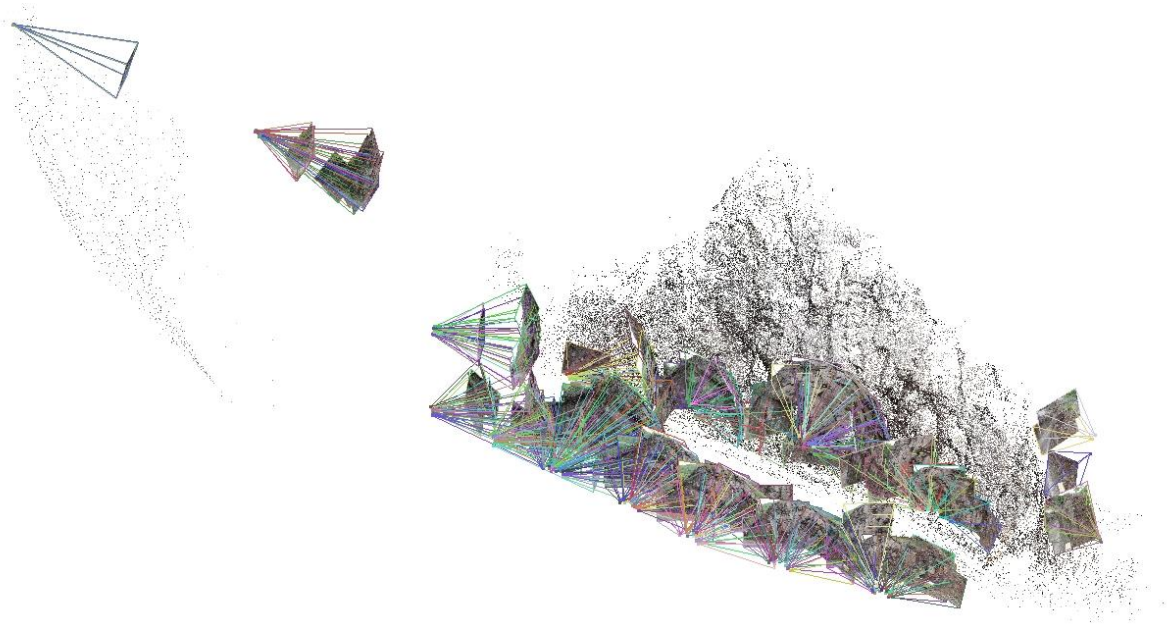

Figure 45: Camera positons for the outcrop Alte Sarnerstrasse 2, on the top left side the additional camera angle is well visible, and on the left edge some sparse point are visible, that went cut out for the later work with the point cloud.

The positioning for the pictures was chosen differently, to see if that impacts the result. Similarly to the outcrop Halbweg the pictures were shot from (~15) different standpoints (Fig. 45) in an all-around-view. In addition to that for this outcrop it was possible to take pictures from an elevated point of view, since it is located on the bottom side of a hairpin bend. These additional pictures allow getting a good view on the shallow angled joints further up the outcrop.

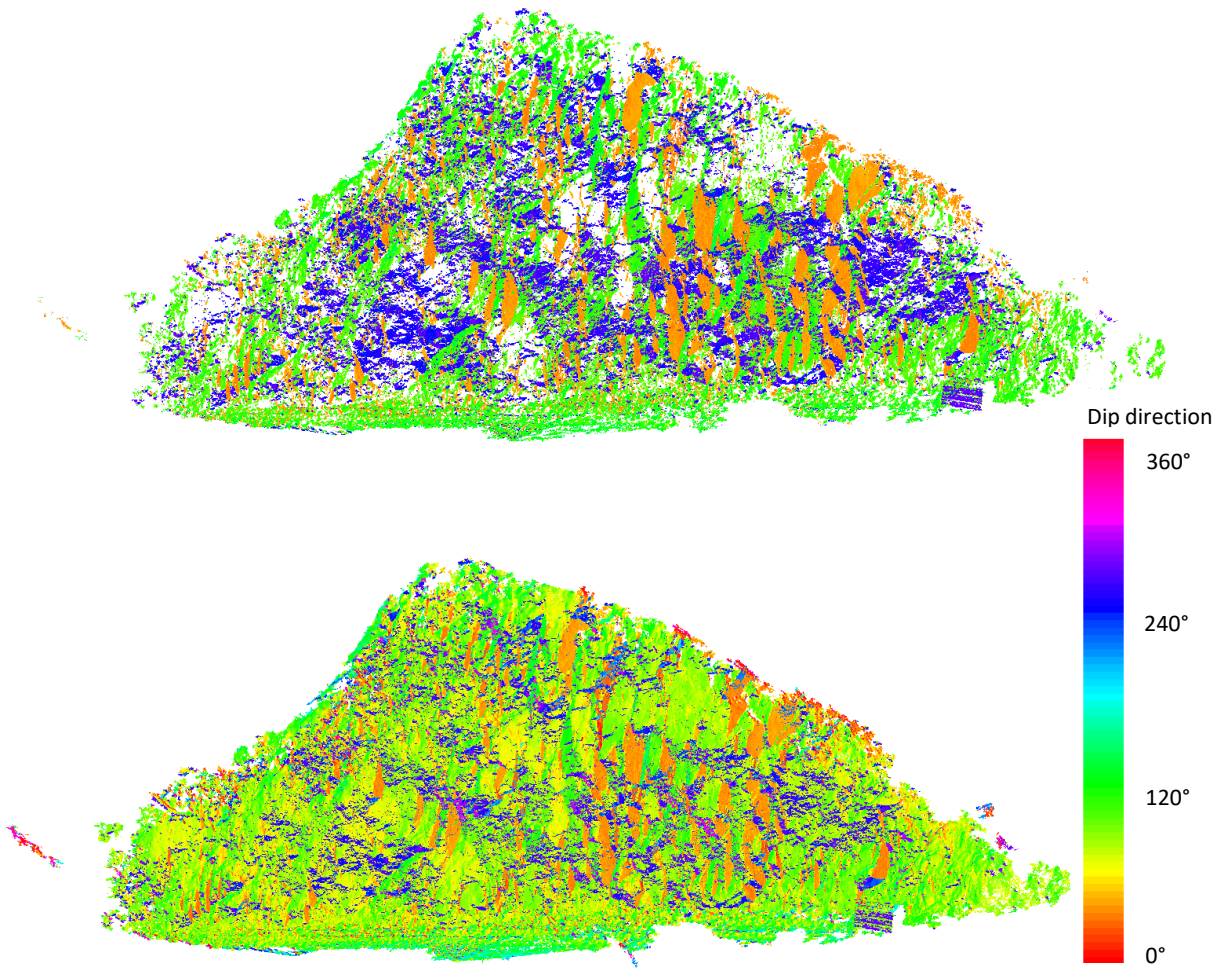

Figure 46: Comparison of the information given by the scalar field. On the bottom there is the full spectrum of dip-directions for the cloud. On top are the three sets extracted from the whole cloud. On a special note: it's important to not use the information of the wooden box, which is also clearly visible in both point clouds

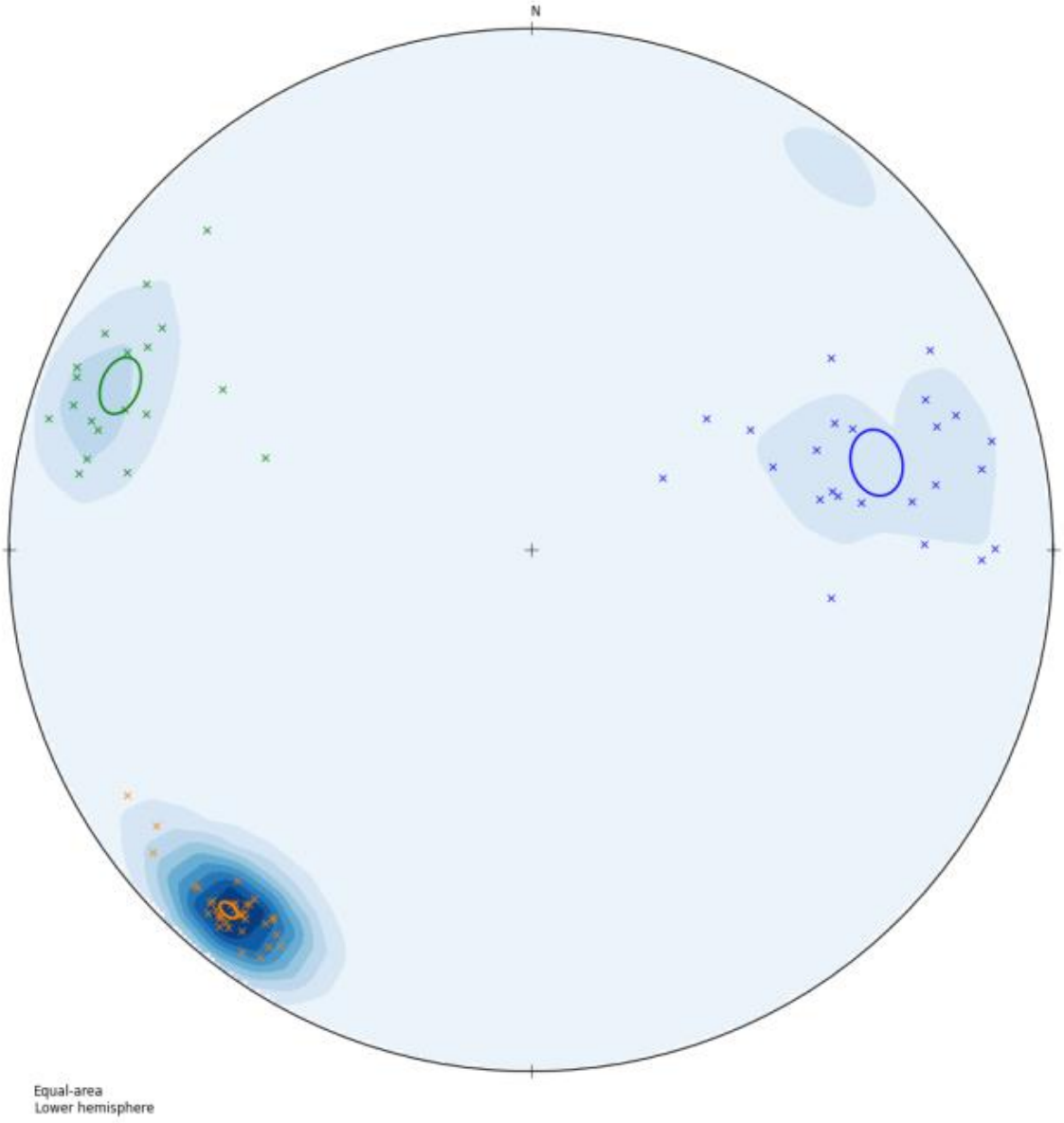

Figure 47: Stereographic plot of the measured orientations
Set 1: Orange
Set: 2 Green
Set 3: Blue

The comparison of the two outcrops Alte Sarnerstrasse 1 (lower position) and Alte Sarnerstrasse 2 (upper Position) (Fig. 41 and Fig 46) shows, that the orientation of the sets is not quite the same. This is also visible when comparing the stereographic plots; Fig. 43 with fig 47. Set 1 (orange) is a lot steeper in the outcrop 1. Also the set 2 (purple) and 4 (blue) of the outcrop alte Sarnerstrasse seem so blend together in the upper outcrop forming the set 3 (blue) of the outcrop alte Sarnerstrasse 2. Meanwhile the set 5 is not appearing at all. This is most likely explained by the fact that, the set 5 is also only appearing in the lower outcrop next to the drainage duct (Fig. 41)

The parameters of the rock structure of each set will be presented in Chapter 3.6

3.5. Computing efficiency

An interesting point to keep track off, is the time management for the calculations. Since the acquired data quickly stacks up and starts to get computation heavy.
All the office work was done on a windows 10 home (64bit) system, running on an Intel ® Core ™ i7-770 CPU @ 3,60GHz; using 16 GB of RAM.

Outcrop	Pictures used	Time spend			Points in Pointcloud
		sfm; mssing matches	3D compution	time for sfm dense	
Alte Sarnerstrasse_1	199	52 min	220sec	92 min	12846721
Halbweg	258	52 min	156sec	74 min	9468120
Alte Sarnerstrasse_2	207	56 min	187sec	83 min	14023105
Windlahn	174	37 min	153sec	60 min	8001328
Alte_Sarnerstraße_1_150pics	150	25 min	130sec	73 min	10106003
Alte_Sarnerstraße_1_100pics	100	9 min	97sec	40 min	6582516

Table 1: Comparison of the used pictures and the time spent computing the dense point cloud

The table 1 shows that the time for finding missing matches increases a lot with the amount of pictures used, for example the increase of the Alte Sarnerstrasse 1, using 100 pictures (under 10 mins) goes up more than 5times for the 200 pictures.
The Table 1 also shows that there is no correlation between the pictures used and the time spent to create the dense point cloud, a better fit would be the time needed for the amount of points created (Fig. 48). For the few tests done, this seems to be a linear correlation; meaning that even a lot more points won't increase the calculation time exceedingly.
But this data is insufficient and will most likely change when the clouds reach a lot bigger dimensions.

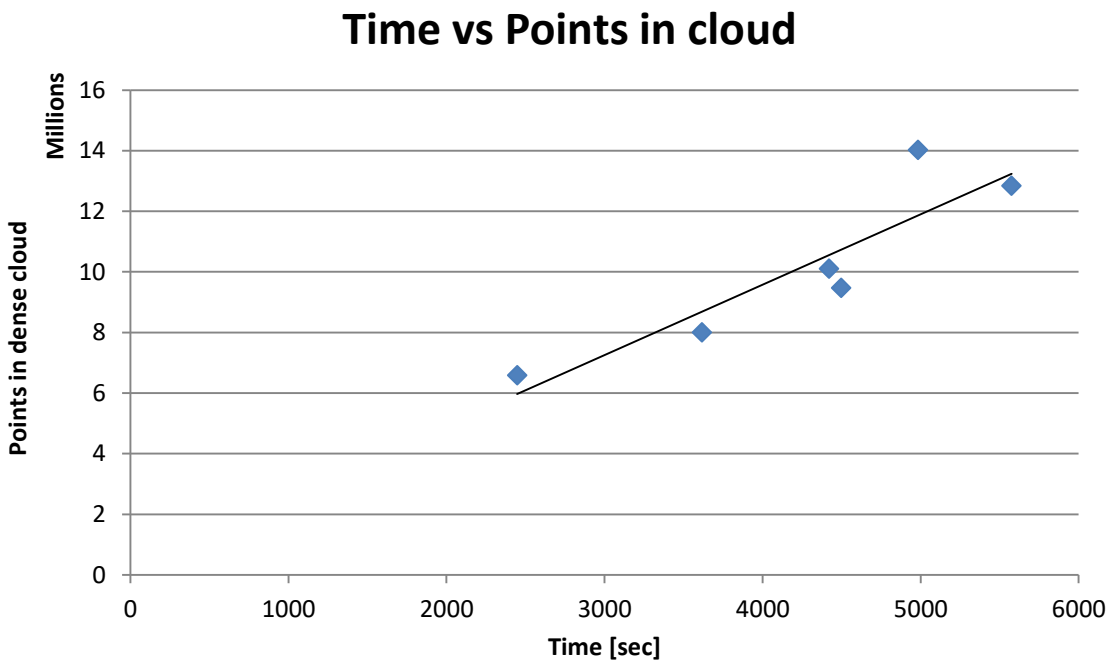

Figure 48: Time needed for the dense cloud reconstruction plotted vs the amount of points of that cloud

3.6. Statistical parameters of all outcrops

Thanks to the open source software Openstereo Grohman et al. (2010) it is possible to extract valuable information about the statistic accuracy of the information gathered from the point clouds. Most importantly the information about the mean dip and dip direction, but also the information about the radius of the cone of confidence gives a good idea on the distribution of the discontinuities in the field. This information has to be kept in mind during the gathering the data from the point cloud. Because this tool allows to measure all surfaces of one set, should there be a bigger variation of the dip and dip direction in the field (and therefore in the measurements) this variation shows up with a bigger radius of the circle of confidence.

Another aspect playing a part in the same problem is the fact of the sample size, the compass plug-in allows resizing the measuring tool; a small sample size maybe prone of surface roughness, whilst large sampling areas might cover parts of the point cloud that are not actually part of the discontinuity surface, see Fig 49.

This is also a form of bias to keep considering (see Chapter 2.1.3), to minimize the effect of that, for all sets of all outcrops there were at least representative 10 measurements for each set, usually being more than 30.

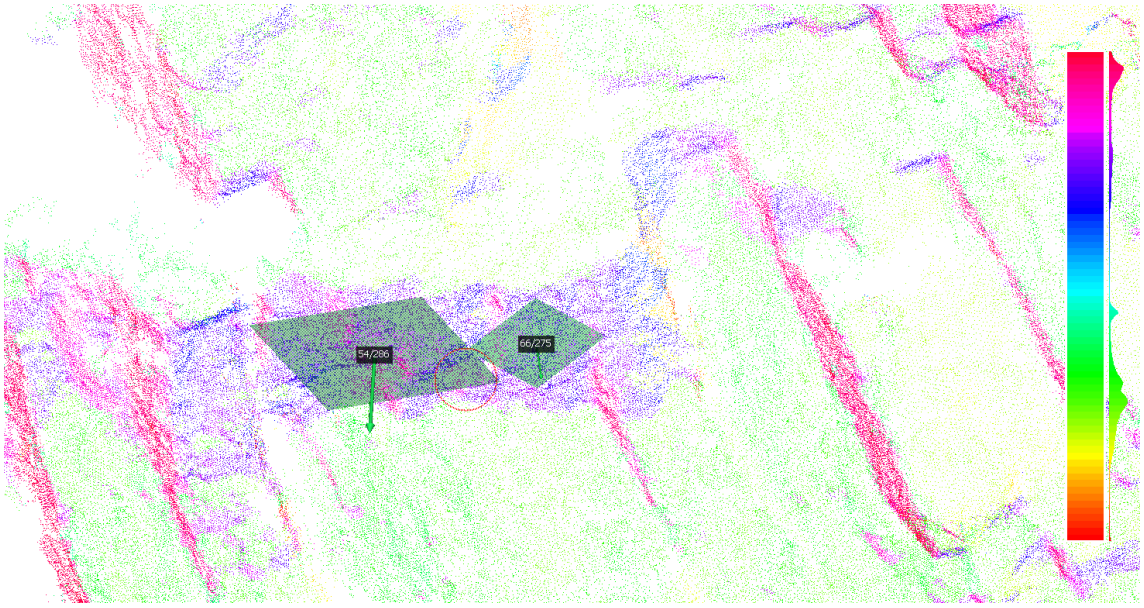

Figure 49: Two orientation measurements with different sample size using Cloud Compare compass on the same discontinuity surface, the left measurement with a big surface area being 54/286 and on the right with a small sampling area 66/275.

3.6.1. Results of orientation measurements

Outcrop		n	Dipdir	dip	Radius of confidence at 5%
Windlahn	Set 1	16,00	104,10	73,90	1,99
	Set 2	12,00	256,30	45,20	4,33
	Set 3	22,00	345,50	80,20	2,96
	Set 4	10,00	65,00	72,90	2,32
Halbweg	Set 1	32,00	22,60	72,50	2,25
	Set 2	28,00	297,20	76,90	3,38
	Set 3	19,00	101,60	39,30	6,96
Alte Sarnerstraße	Set 1	81,00	28,00	51,50	2,81
	Set 2	28,00	272,80	70,80	1,91
	Set 3	20,00	181,10	68,80	3,93
	Set 4	50,00	229,90	70,40	3,20
	Set 5	22,00	319,50	80,00	4,31
Alte Sarnerstraße 2	Set 1	71,00	40,00	79,20	1,23
	Set 2	38,00	111,80	73,70	3,67
	Set 3	48,00	225,80	57,80	4,55

Table 2: Results gained from the open-source software Openstereo

Outcrop	mean dipdirection/dip	spacing ± 10cm	Notes	Setcolour (CloudCompare)
Halbweg				
Set 1	22/70	95		orange
Set 2	297/76	210 (very persistent)	50 (not very persistent)	violett
Set 3	121/30	140		grün
Outcrop	mean dipdirection/dip	spacing ± 5cm		
Alte Sarnerstrasse 1		[cm]		Colour (CloudCompare)
Set 1	27/51	10		gelb/orange
Set 2	272/70	30		violett
Set 3			Set was removed due to its similar orientation to set 2 and 4	cyan
Set 4	230/70	15		Blau
Set 5	319/79	10		Magenta
Outcrop	mean dipdirection/dip	spacing ± 5cm		
Alte Sarnerstrasse 2		[cm]		Colour (CloudCompare)
Set 1	40/79	12		orange
Set 2	111/73	15		grün
Set 3	255/57	estimated 15	outcrop surface almost parallel to discontinuities	blau
Outcrop	mean dipdirection/dip	spacing ± 10cm		Colour (CloudCompare)
Windlahn		[cm]		
Set 1	102/72	70		grün
Set 2	261/44	55		blau
Set 3	345/76	60	+ additional every 15 smaller ones	magenta
Set 4	64/75	420	+ additional every 50	gelb

Table 3: Overview of the results from the measurements inside CloudCompare

3.7. Comparison of the way the pictures were taken

One of the find outs, is the fact that taking the pictures perpendicular to the surface generally generates slightly better point clouds when comparing the amount of points in the final point cloud with the amount of pictures used as input, for example when comparing the outcrop Alte Sarnerstrasse 1 with 199 pictures resulting in roughly 13 Mio. point cloud, with the outcrop Halbweg where 258 pictures resulted in a 9 Mio. point cloud (Table 1).

Both having roughly similar outcrop dimensions, with to biggest difference being the approach the pictures were taken. Nevertheless this difference can be also caused partly by many other influences on the outcrop, for example different surfaces and vegetation influencing the amount of recognized tracks during the SfM workflow.

Another advantage of taking the pictures stepwise is the possibility selecting pictures to erase to reduce the overall calculation time; with hundreds of pictures a specific detail or part of the outcrop can be ignored when deleting the pictures capturing it, on the contrary on the approach where the outcrop was captured on a few standing points, the entire outcrop will appear on all standing points, and its rather difficult to specifically delete one uninteresting part.

Generally speaking both approaches fulfil the task to generate a usable point cloud, but the approach of taking pictured perpendicular seems to be winning when it comes to time management, while providing better (denser) point clouds.

4. Discussion

The results of the workflow are really consistent and make a good picture of the actual situation in the field. The thesis shows the great use and applicability of this form of photogrammetry for the everyday work of a geologist. Of special interest are the results of the quote on quote easier outcrops, like Windlahn (Chapter 3.1) with large discontinuity surfaces. This kind of outcrop would also be easier for the traditional scanline approach, but considering not all outcrops are located next to a street, the SfM workflow would generate similar quality results if the outcrop was not easily reachable by foot, or not save enough to put a scanline.

Another very important point is the fact this study revealed that the entire workflow is easily executable with the existing open source software. With little learning effort they provide great results, which make this workflow especially interesting for low-budget projects and also for young geologists doing their fieldwork for big companies. The fact that all the work can be reproduced and revisited, allows other experts to take a look on the situation in-situ and interpreting the gathered data tinker together on possible future steps.

Testing the repeatability of the workflow with using the same pictures like for the outcrop Halbweg showed great results, but also reducing the amount of images used like for the outcrop Alte Sarnerstrasse lead to good results. The transformation matrix of both examples showed a great overlap, meaning that this workflow can be redone at any given moment, without changing the results significantly.

This study steps in between the many studies using photogrammetry for surface reconstruction for example Eltner et al. (2015) and tries to link it to the applied work of a engineering geologist trying to describe rock mass properties.

The pain-point of the whole process is the data extraction from the point cloud, although CloudCompare provides a lot of good tools and offers a well-functioning platform; the data cannot be extracted automatically. The knowledge and expertise of a trained geologist is still needed to fulfil that task. Nevertheless the program creates a great basis for interpreting the point cloud, with many valuable tools to use. Probably the most important, is still the 3D vision of the outcrop with RGB combined with the scalar field displaying the dipdirection, by turning them on and off it is easy to distinguish the different discontinuities on the screen. In addition to that this also allows to rotate and zoom to parts of the outcrop that otherwise might be overseen or not noticed due to a bad exposure or small size.

5. Conclusions

The process of gathering valuable information for describing rock masses by photogrammetry works well for small outcrops like shown in this work. Depending on the accuracy of the GPS measurement and the initial measurements of the ground control points (GCPs) the method shows great results.

The execution of the workflow is rather simple, yet it is important to keep in mind what aspects of the field work will later on influence the quality of the point cloud, like lighting or camera positioning. As for this few examples, the best way to take pictures is head-on with a small distance towards the surface and roughly 1m wide sidesteps. The amount of pictures needed is definitely dependent on the surface area and on the texture (roughness), but as shown for the outcrop Alte Sarnerstrasse, even when reducing the pictures down to 100 the resulting point cloud still gives reasonable results when it comes to orientation and spacing measurements.

The vegetation didn't cause that many problems for this kind of outcrops, since due to the origin of the rock masses, the discontinuities are rather sharp and well defined, forming mostly large, uniformal surfaces. Therefore each surface was rather easy to define and gather information from it.

The aspect of time was an interesting point to take into consideration, since the field work was done usually in less than 1hour for each outcrop. Depending on the needed accuracy the later workflow was also completed very fast, around 1-2hours of calculation time. The extraction of the information of the point clouds still needs some experience and basic knowledge in geology, since it is very important to select the right surfaces for each set and to put the data from the field into a reasonable model, to represent reality as good as possible.

On a final note it is important to mention the importance of the pictures themselves; they are a good snapshot of the actual situation of the outcrop. This information can be used later on, if there are any movements or changes, it would be easy to compare a new point cloud with the gathered data, to create sort of an archive of the outcrop. Additionally this workflow enable multiple people to watch the outcrop in a 3D environment without being physically there. This allows discussions and insights from other people, while providing actual data, being visible and processed, and not just verbal descriptions and 2D pictures as it stands until now.

As a further step of investigation could an analysis using (key-) block theory Goodman (1995). This would allow providing an in-depth understanding of possible keyblocks from the

gathered data, in a very safe and efficient way.

A fantastic way to use this additional step would be for tunnelling or mining. In this environment it is crucial to get information as fast and safe as possible. It would be a great tool to go in and take pictures within a few minutes after a blast and then moving out, back into a safe space, to process the pictures and create the geotechnical model needed to keep on working.

All things considered the SfM workflow is a valuable tool to gather information about outcrops and their properties, even more so, considering the entire workflow being executable with open-source-software. This opens the concept also for a broad variety of users, depending on the accuracy needed it can be used to describe a single outcrop for a geological report, or for large project with many iterations used, for example tunnelling.

As another future research idea could be to see if the roughness of discontinuities can be measured by using the same workflow. Or if it is possible to extract it from the information gained by the stereonet-plots, since rougher surfaces most likely would show a bigger variation in the measurements and therefore create a bigger cone of confidence.

6. Bibliography

Allmendinger, R.W., Cardozo, N. and Fisher, D., 2012. Structural geology algorithms: Vectors and tensors in structural geology*: Cambridge University Press (book to be published in early 2012).*

Bargossi, G.M., Bove, G., Cucato, M., Gregnanin, A., Morelli, C., Moretti, A., Poli, S., Zanchetta, S. and Zanchi, A. 2011. Erläuterungen zur Geologischen Karte von Italien im Maßstab 1:50000, Blatt 013 Meran, *Servizio geologico d'Italia (ISPRA)*

Bemis, S., Micklethwaite, S., Turner, D., James, M., Akciz, S., Thiele, S. and Bangash, H. 2014. Ground-based and UAV-Based photogrammetry: A multi-scale, high-resolution mapping tool for Structural Geology and Paleoseismology. *Journal of Structural Geology.* Vol. 69. pp 163-178

Brandner, R., Gruber, A. and Keim, L. 2007. Geologie der westlichen Dolomiten: Von der Geburt der Neothethys im Perm zu Karbonatplattformen, Becken und Vulkaniten der Trias. *Geo.Alp, Volume 4*, pp 95-121

Brandner, R., Gruber, A., Morelli C and. Mair, V. 2016. Pulses of Neothethys-Rifting in the Permomesozoic of the Dolomites. *Geo.Alp, Volume 13*, pp 7-70

Boulch, A. and Marlet, R, 2012. Fast and Robust Normal Estimation for Point Clouds with Sharp Features. *Eurographics Symposium on geometry Processing*, Volume 31, Number 5

Cardozo, N. and Allmendinger, R.W., 2013. Spherical projections with OSXStereonet: *Computers & Geosciences, volume. 51,* pp 193–205

Carrivick, J.L., Smith, M.W. and Quincey, D.J. 2016. Structure from motion in the geosciences. New York, *NY: John Wiley & Sons*

Cotza, G. 2009. Geologische und geotechnische Verhältnisse der Massenbewegungen bei Pontives (Gadertal, Südtirol), Universität Wien

James, M.R. and Robson, S. 2012. Straightforward reconstruction of 3D surfaces and topography with a camera: Accuracy and geoscience application. *J. Geophys. Res.*, Vol. 117, F03017, doi:10.1029/2011JF002289

Eltner, A. and Schneider, D. 2015. Analysis of different methods for 3D reconstruction of natural surfaces from parallel-axes UAV images. *The photogrammetric record 30 (151),* pp 279-299

Falkingham, P.L. 2014. Acquisition of high resolution three-dimensional models using free, open-source, photogrammetric software*, Palaeontologia Electronica,* Vol. 15, Issue 1; 1T:15p;

Fisher, R., Perkins, S., Walker, A. and Wolfart E. 2000. HYPERMEDIA IMAGE PROCESSING REFERENCE**,** *https://homepages.inf.ed.ac.uk/rbf/HIPR2/gsmooth.htm (last access 14.11.2019)*

Furukawa, Y. and Ponce, J. 2010. Accurate, Dense and Robust Multi-View Stereopsis. *IEEE Transactions on Pattern Analysis and Machine Intelligence,* Vol 32, pages 1362–1376.

Furukawa, Y. and Ponce, J. 2007. Accurate, Dense, and Robust Multi-View Stereopsis, *IEEE Computer Society Conference on Computer Vision and Pattern Recognition*

Furukawa, Y., Curless, B., Seitz, S.M. and Szeliski, R. 2010. Towards Internet-scale Multi-view Stereo, *Computer Vision and Pattern Recognition*

González-Matesanz, J., Dalda, A., Quirós, R. and Celada, J. 2003. ED50-ETRS89 Transition models for the Spanish Geodetic Network.

Goodman, R.E., 1995. Block Theory and its application, *Géotechnique 45, No. 2*, pp 383-423

Grohmann, C.H. and Campanha, G.A.C., 2010. OpenStereo: open source, cross-platform software for structural geology analysis. *Presented at the AGU 2010 Fall Meeting, San Francisco, CA.*

Grohmann, C.H., Campanha, G.A.C. and Soares Junior, A.V., 2011. OpenStereo: um programa Livre e multiplataforma para análise de dados estruturais. *XIII Simpósio Nacional de Estudos Tectônicos.*

Hartley, R.I. and Zisserman, A. 2004. Multiple View Geometry in Computer Vision. *Cambridge University Press*

Haneberg, W., Norrish, N. and Findley, D. 2006. Digital outcrop characterization for 3-D structural mapping and rock slope design along Interstate 90 near Snoqualmie pass, Washington. *Proceedings 57th, Annual Highway Geology Symposium, Breckenridge, Colorado*

Heng, P.B.C., Chandler J., H. and Armstrong, A. 2010. Applying close range digital photogrammetry in soil erosion studies*. The Photogrammetric record 25 (131)*. pp 240-265

Hudson, J. A and Harrison, J. P.1992. A new approach to studying complete rock engineering problems*, Quarterly Journal of Engineering Geology and Hydrogeology, 25*, pp 93-105

Lato, M.J. and Vöge, M. 2012. Automated mapping of rock discontinuities in 3D lidar and photogrammetry models. *International Journal of Rock Mechanics & Mining Sciences, Volume 54,* pp 150-158

Le Maitre, R.W., Streckeisen, A., Zanettin, B., Le Bas, M.J., Bonin, P., Bateman, G., Bellieni, G., Dudek, A., Efremova, S., Keller, J., Lamyre, J., Sabine, P.A., Schmid, R., Sørensen, H., Woolley, A.R. 2002 Igeneous Rocks Aclassification and Glossary of Terms. Cambridge University Press

Liu, Q. 2018. Gebirgscharakterisierung, *Technische Universität Graz*, unpublished

Longuet-Higgins, H.C. 1981. A computer algorithm for reconstructing a scene from two projections, *Nature, Vol 293*, pp 131-135

Lourakis, A.M.I., Argyros, A.A. 2009. SBA: A Software Package for Generic Sparse Bundle Adjustment, *ACM Trans. Math. Software Vol. 36,* pp. 1-30

Lowe, D.G. 2004. Distinctive Image Features from Scale-Invariant Keypoints, International *Journal of Computer Vision*, Volume 60, pp 91–110

Marocchi, M., Morelli, C., Mair, V., Klötzli, U. and Bargossi, G.M. 2008. Evolution of Large Silicic Magma Systems: New U-Pb Zirkon Data on the NW Permian Athesian Volcanic Group (Southern Alps, Italy). *Journal of Geology, Volume 116,* pages 480-498

Morelli, C., Avanzini, M., Bargossi, G.M., Cucato, M., Prosser, G. and Tomasoni, R. 2013. Geologischer Exkursionsführer Blatt 026 Eppan, *Amt für Geologie und Baustoffprüfung Autonome Provinz Bozen-Südtirol*

Mosbrucker, A.R., Major, J.J., Spicer, K.R. and Pitlick, J. 2017. Camera system considerations for geomorphic applications of SfM photogrammetry. *Earth Surface Processes and Landforms*, Volume 42, pp 969-986

Remondino, F. 2006. Detectors and descriptors for photogrammetric applications, International Archives of Photogrammetry, *Remote Sensing and Spatial Information Sciences,* Volume 36, pp 49–54

Remondino, F. and El-Hakim, S. 2006. Image-Based 3D Modelling: A Review. *The Photogrammetic record 21 (115)*, pp 269-291

Snavely, K.N. 2008. Scene Reconstruction and Visualization from Internet Photo Collections, *University of Washington*

Snavely ,N., Seitz, S.M. and Szeliski, R. 2006. Photo Tourism: Exploring image collections in 3D, *ACM Transactions on Graphics (Proceedings of SIGGRAPH 2006)*

Snavely ,N., Seitz, S.M. and Szeliski, R. 2007. Modeling the World from Internet Photo Collections. *International Journal of Computer Vision*

Thomas, H. and Cantré, S. 2009. Applications of low-budget in the geotechnical laboratory, *The photogrammetric record 24 (128)*, pp 332-350

Triggs, B., McLauchlan, P., Hartley, R. and Fitzgibbon, A. 2000. Bundle Ajustment – A ModernSynthesis. Bill Triggs and Andrew Zisserman and Richard Szeliski. *Vision Algorithms: Theoryand Practice, 1883, Springer-Verlag,* pp 298–372

Watkins, H., Bond, C., Healy, D. and Butler, R.W.H. 2015. Appraisal of fracture sampling methods and a new workflow to characterise heterogeneous fracture networks at outcrop. *Journal of Structural Geology. 84.*

Westoby, M.J., Brasington, J., Glasser, N.F., Hambrey, M.J. and Reynolds, J.M., 2012. 'Structur-from-Motion' photogrammetry: A low-cost, effective tool for geoscience applications, *Geomorphology 179,* pp 300-314

Wu, C., 2013. Towards Linear-time Incremental Structure From Motion, 3DV

Wu, C., Agarwal, S., Curless, B. and Seitz, S.M. 2011. Multicore Bundle Adjustment, CVPR

Wu, C., 2007. SiftGPU: A GPU implementation of Scale Invaraint Feature Transform (SIFT)",http://cs.unc.edu/~ccwu/siftgpu